



**RETURNING MATERIALS:**  
Place in book drop to  
remove this checkout from  
your record. FINES will  
be charged if book is  
returned after the date  
stamped below.

--	--	--

PHASE TRANSFORMATIONS IN  $(\text{Ni,Cu})_3\text{Sn}$  ALLOYS

BY

Jung-soon Lee Pak

A DISSERTATION

submitted to  
Michigan State University  
in partial fulfillment of the requirements  
for the degree of

DOCTOR OF PHILOSOPHY

Department of Metallurgy, Mechanics and Materials Science

1987

## ABSTRACT

### PHASE TRANSFORMATIONS IN $(\text{Ni,Cu})_3\text{Sn}$ ALLOYS

BY

Jung-soon Lee Pak

The phase transformations in  $(\text{Ni,Cu})_3\text{Sn}$  alloys containing Cu contents ranging between 10 and 22 at% were investigated in detail by means of optical and scanning and transmission electron microscopy, electron and X-ray diffraction techniques, and differential thermal analysis. A high-temperature  $\text{DO}_3$  phase was transformed to an ordered 2H (beta- $\text{Cu}_3\text{Ti}$ -type) orthorhombic phase at a temperature of around  $700^\circ\text{C}$  in alloys containing Cu contents between 14 and 20 at%. Residual areas of the  $\text{DO}_3$  phase then were transformed to both the 2H phase and a new phase at around  $460^\circ\text{C}$ . Electron and X-ray diffraction analyses revealed that the new phase exhibited a triclinic structure, slightly distorted from the 2H structure. Below that temperature, the three phases of  $\text{DO}_3$ , 2H, and d2H are present. These results were consistent with those obtained from specimens containing 20 at% Cu, aged at various temperatures.

Transmission electron microscope observations of specimens with Cu contents of 14, 17.5, and 20 at%, furnace-cooled from  $1000^\circ\text{C}$ , demonstrated that the d2H phase exhibited acicular structures containing a large number of uniformly distributed internal faults. These

Jung-soon Lee Pak

d2H structures are surrounded by the 2H phase, which contains rod-shape structures having (101) faults and a low density of dislocations.

TEM observations of specimens quenched from 1000°C to ice water revealed that the high-temperature  $DO_3$  phase was retained for alloys containing Cu ranging from 16 and 22 at%. For an alloy with a Cu content of 14 at%, a 2H martensite was formed containing (121) twins.

A new phase diagram is proposed for the  $(Ni,Cu)_3Sn$  alloys in the range of Cu between 10 and 22 at%. This phase diagram is different from the one found in literature, showing a single phase of 2H at temperatures below about 900°C in the range of Cu contents between 8 and 18 at%. It is also proposed that the d2H phase can be formed from an  $L2_1$  phase via the  $DO_3$  phase.

## ACKNOWLEDGMENTS

My sincere thanks go to Professor K. Mukherjee, my advisor, for his stimulating presence throughout this work and for his understanding of my being on leave from MSU to pursue part of this work.

To Professor O.T. Inal, my coadvisor, for his encouragement to complete this work.

To Professor G. Purcell for allowing me to use his research facilities in the Department of Materials and Metallurgical Engineering, New Mexico Institute of Mining and Technology.

To Dr. S. Sirkar for his help in the DTA experiments.

My special thanks go to my husband, Han, and my parents, Mr. and Mrs. H. Lee for their high inspiration and continued interest in my work.

To my son, Yune, for his stay in East Lansing with me from the fall of 1985 to the spring of 1986.

## TABLE OF CONTENTS

	Page
LIST OF TABLES.....	vi
LIST OF FIGURES.....	vii
CHAPTER 1	INTRODUCTION
1.1	Introduction..... 1
1.2	Martensitic Transformations in $DO_3$ Ordered Alloys..... 3
1.3	Massive Transformations in Cu-based Alloys..... 11
1.4	The $Ni_3Sn$ System..... 17
1.5	The $(Ni,Cu)_3Sn$ System..... 23
CHAPTER 2	OUTLINE OF THE PRESENT WORK..... 26
CHAPTER 3	EXPERIMENTAL PROCEDURES..... 28
3.1	Preparation and Heat Treatment of Alloys..... 28
3.2	Optical Microscopy, X-ray Diffraction, and Scanning and Transmission Electron Microscopy..... 30
3.3	Differential Thermal Analysis..... 32

TABLE OF CONTENTS--continued

	Page
CHAPTER 4	EXPERIMENTAL RESULTS AND DISCUSSIONS
4.1	Optical and Scanning Electron Microscopy..... 33
4.2	Results of Diffractometer and Debye- Scherrer Methods..... 41
4.3	Microstructures of Furnace-cooled (Ni,Cu) <sub>3</sub> Sn Alloys..... 58
4.4	Microstructure and Crystal Structure of As-quenched (Ni,Cu) <sub>3</sub> Sn Alloys.... 87
4.5	Aging Effects of the Ni-20Cu-25Sn Alloy..... 92
4.6	Differential Thermal Analyses.....106
4.6.1	Results and Discussion.....106
4.6.2	Conclusions.....110
CHAPTER 5	DISCUSSION
5.1	A Proposed Phase Diagram of the (Ni,Cu) <sub>3</sub> Sn System.....112
5.2	A Formation Mechanism of a Distorted 2H Phase.....116
CHAPTER 6	SUMMARY AND CONCLUSIONS.....124
REFERENCES.....	127

## LIST OF TABLES

TABLE	Page	
4.1	Angles and intensities of reflection peaks for a 2H-orthorhombic structure of a furnace-cooled Ni-14Cu-25Sn alloy. Lattice parameters used for theoretical calculation: $a=4.510$ , $b=5.393$ , $c=4.300\text{\AA}$ ; Cu-k alpha: $1.544390\text{\AA}$ ; Debye-Scherrer method used.....	43
4.2	Angles, d-spacings, and intensities of reflection peaks for a $DO_3$ structure of a Ni-17.5Cu-25Sn alloy. Lattice parameter used: $a=5.910\text{\AA}$ ; Cu-k alpha: $1.54439\text{\AA}$ ; Debye-Scherrer method used.....	49
4.3	Angles and intensities of reflection peaks for a $DO_{19}$ structure of a furnace-cooled Ni-14Cu-25Sn alloy. Lattice parameters used for theoretical calculation: $a=b=5.306$ , $c=4.260\text{\AA}$ ; Cu-k alpha: $1.544390\text{\AA}$ ; Debye-Scherrer method used.....	50
4.4	Debye-Scherrer data obtained from the alloys, furnace-cooled from $1000^\circ\text{C}$ . Cu-k alpha used.....	55
4.5	D-spacings of the d2H phase.....	85
4.6	Angles between two planes for d2H and 2H structures.....	86
4.7	X-ray reflection peaks observed in a specimen aged 24hr at $500^\circ\text{C}$ .....	95
4.8	X-ray reflection peaks observed in a specimen aged 24hr at $600^\circ\text{C}$ .....	97
4.9	Summary of DTA analyses obtained from as-quenched $(\text{Ni,Cu})_3\text{Sn}$ specimens.....	108
5.1	Examples of tetragonally distorted CsCl-type compounds.....	123

## LIST OF FIGURES

FIGURE		Page
1.1	Unit cell of $DO_3$ - and $L2_1$ -type superlattices...	5
1.2	Two kinds of atomic layers, A and B, in (110) planes of $DO_3$ structure.....	6
1.3	Six kinds of atomic layers in close-packed structures of martensite transformed from $DO_3$ -type superlattice. The arrows indicate the displacement vector of each layer referred to layer A.....	7
1.4	Unit cell of 2H (beta- $Cu_3Ti$ -type) superlattice.	8
1.5	Stacking sequence of basal planes for a 9R structure.....	10
1.6	A portion of a phase diagram in the Cu-Ga system.....	13
1.7	Lattice parameters of $\xi$ , $\xi'$ , and $\xi_m$ phases in the Cu-Ga system.....	15
1.8	Phase diagram of Ni-Sn system.....	18
1.9	Atomic arrangements in the (0001) plane of $DO_{19}$ structure (a) and in the (001) plane of 2H structure (b).....	21
1.10	Phase diagram of Ni-xCu-25Sn alloys.....	24
3.1	Flow chart of heat treatments employed.....	29
4.1	Microstructure of a Ni-14Cu-25Sn alloy, furnace-cooled from 1000°C to room temperature.....	34
4.2	Microstructure of a Ni-14Cu-25Sn alloy, furnace-cooled from 1000°C to room temperature.....	35

LIST OF FIGURES--continued

FIGURE	Page
4.3 Scanning electron micrographs of a Ni-14Cu-25Sn alloy, furnace-cooled from 1000°C.....	37
4.4 Microstructure of a Ni-17.5Cu-25Sn alloy, furnace-cooled from 1000°C.....	39
4.5 Microstructure of a Ni-20Cu-25Sn alloy, furnace-cooled from 1000°C.....	40
4.6 Partial diffractometer pattern of a furnace-cooled Ni-17.5Cu-25Sn alloy.....	42
4.7 Composition dependence of the lattice parameter of DO <sub>3</sub> structure in as-quenched Ni-xCu-25Sn alloys.....	48
4.8 Partial diffractometer pattern of a furnace-cooled Ni-14Cu-25Sn alloy.....	53
4.9 Partial diffractometer pattern of a furnace-cooled Ni-20Cu-25Sn alloy.....	54
4.10 Microstructure of a Ni-14Cu-25Sn specimen, furnace-cooled from 1000°C. (a) bright field image of 2H and d2H phases. (b) diffraction pattern, taken from the top left-hand side of a 2H region: [1 $\bar{1}$ 1] zone axis. (c) diffraction patterns, taken from the central region of the micrograph: [1 $\bar{1}$ 1] zone axis for 2H and d2H. (d) angles between two reflection spots.....	60
4.11 Enlarged micrograph of an area indicated by the single-headed arrow in Figure 4.10.....	62
4.12 Enlarged micrograph of an area indicated by the double-headed arrow in Figure 4.10. Note fringes of stacking faults and dislocation networks in a 2H region.....	63

LIST OF FIGURES--continued

FIGURE	Page
4.13 High magnification micrograph of a furnace-cooled Ni-14Cu-25Sn specimen, showing many microstructural features.....	64
4.14 Microstructure of a Ni-14Cu-25Sn specimen, furnace-cooled from 1000°C. (a) bright field image of 2H and d2H phases. (b) diffraction pattern of $[2\bar{3}4]$ zone axis taken from a 2H region. (c) diffraction patterns taken from a two-phase region.....	68
4.15 Microstructure of a Ni-14Cu-25Sn specimen, furnace-cooled from 1000°C. (a) bright field image of 2H and d2H phases. (b) diffraction pattern taken from an area containing bands....	70
4.16 High magnification micrographs taken, (a) from area A; (b) from area B; and (c) from area C in Figure 4.15.....	71
4.17 Electron micrograph of a 2H region taken from a Ni-14Cu-25Sn specimen, furnace-cooled from 1000°C. Note (101) planar faults.....	75
4.18 Bright field image of a Ni-20Cu-25Sn specimen, furnace-cooled from 1000°C to room temperature. Note dislocations and planar faults in 2H regions and planar faults in d2H regions.....	77
4.19 Bright field image of a Ni-20Cu-25Sn specimen, furnace-cooled from 1000°C, showing zigzag bands.....	78
4.20 Bright field image of a Ni-20Cu-25Sn specimen, furnace-cooled from 1000°C to room temperature. Note many dislocation loops and dislocation lines in 2H regions.....	80

LIST OF FIGURES--continued

FIGURE	Page
4.21 Electron diffraction patterns taken from 2H areas of Ni-14Cu-25Sn specimens furnace-cooled from 1000°C. Zone axes: (a) [100]; (b) [2̄10]; (c) [01̄1]; and (d) [01̄2].....	82
4.22 Electron diffraction patterns taken from d2H areas of Ni-14Cu-25Sn specimens furnace-cooled from 1000°C. Zone axes: (a) [001]; (b) [010]; and (c) [001] and [2̄14]. ....	83
4.23 Optical micrograph of a Ni-14Cu-25Sn specimen, quenched from 1000°C to ice water, showing a plate-like martensite formed from a DO <sub>3</sub> phase.....	88
4.24 Electron micrograph of a 2H martensite (denoted as 2H') formed in a Ni-14Cu-25Sn specimen, quenched from 1000°C to ice water. Note a high density of (121) twins.....	89
4.25 Microstructure of an as-quenched Ni-14Cu-25Sn specimen, showing two martensite variants containing twins. (a) bright field. (b) diffraction pattern of [1̄20] zone of 2H, taken from an area indicated by the single-headed arrow. (c) diffraction pattern of [1̄24] zone, taken from an area indicated by the double-headed arrow.....	91
4.26 Partial diffractometer pattern of a Ni-20Cu-25Sn alloy, quenched in ice water from 1000°C aged 24 hr at 650°C, and quenched in ice water.....	93
4.27 Partial diffractometer pattern of a Ni-20Cu-25Sn alloy, quenched in ice water from 1000°C aged 24 hr at 500°C, and quenched in ice water.....	96

LIST OF FIGURES--continued

FIGURE	Page
4.28 Partial diffractometer pattern of a Ni-20Cu-25Sn alloy, quenched in ice water from 1000°C, aged 24 hr at 350°C, and quenched in ice water.....	99
4.29 Diffraction pattern of a $[\bar{2}14]$ zone, taken from a d2H region in a Ni-20Cu-25Sn specimen, aged at 350°C for 24 hr.....	100
4.30 Spinodal structure of a Ni-20Cu-25Sn specimen, aged 24 hr at 600°C, following ice-water quenching from 1000°C. (a) modulated structures of a DO <sub>3</sub> phase. (b) two sets of satellite reflections, perpendicular to the modulated structures. Note no satellite of superlattice reflections. [100] zone.....	102
4.31 Phase relationship among M <sub>3</sub> Sn (M=Ni,Cu,Mn) compounds.....	104
4.32 ΔT-vs-T curves measured by a differential thermal analyzer in Ni-xCu-25Sn alloys during a heating process (ΔT: temperature difference). (a) x=14 at%: the starting phase being a quenched 2H martensite; (b) x=17.5 at%: the starting phase being a DO <sub>3</sub> high temperature phase; and (c) x=20 at%: the starting phase being a DO <sub>3</sub> phase.....	107
5.1 A proposed phase diagram for (Ni,Cu) <sub>3</sub> Sn alloys.....	114
5.2 Atomic arrangements of closed-packed planes. (a) the (0001) plane of DO <sub>19</sub> structure. (b) the (001) plane of 2H structure. (c) the (001) plane of d2H structure.....	118
5.3 Schematic illustration describing a formation process of a d2H from DO <sub>3</sub> via L2 <sub>1</sub> .....	121

# 1 INTRODUCTION

## 1.1 Introduction

Some nickel-base ordered alloys are known to show martensitic transformations. Examples are Ni-Al[1,2], Ni-Zn[3,4], Ni-Zn-Cu[5], Ni<sub>3</sub>Sn[6] and (Ni,Cu)<sub>3</sub>Sn[7-9], and Ni-Ti[10]. The Ni-Al, Ni-Zn, and Ni-Zn-Cu alloys all undergo a martensitic transformation from a CsCl(B2)-type ordered cubic phase to an AuCuI(L1<sub>0</sub>)-type ordered tetragonal phase. In the Ni-Al and Ni-Zn-Cu alloys, martensitic transformations are thermoelastic, and these alloys show shape memory effects [1,2,5]. Martensitic transformations in Ni<sub>3</sub>Sn and (Ni,Cu)<sub>3</sub>Sn alloys occur from a beta-Fe<sub>3</sub>Al(DO<sub>3</sub>)-type ordered cubic phase to a beta-Cu<sub>3</sub>Ti(2H)-type ordered orthorhombic phase[6]. A similar martensitic transformation from a DO<sub>3</sub> to a 2H structure also takes place in thermoelastic alloys such as Cu-Ni-Al and Ni-Zn [3,4], which are known to show shape memory effects. Interestingly, the Ni<sub>3</sub>Sn-based alloy does not show any shape memory effect. Since the orientation relationship and habit plane associated with martensitic transformations are essentially the same for the Ni<sub>3</sub>Sn[6], Cu-Ni-Al[11], and Ni-Zn[3,4] alloys, the transformation mechanism is believed to be the same. Thus, the lack of shape memory behavior of a martensite in Ni<sub>3</sub>Sn can not be

explained.

In the past fifteen years, extensive investigations have been carried out to elucidate shape memory mechanisms of shape memory alloys such as Ti-Ni, Cu-Ni-Al, Ag-Cd, and Au-Cd alloys[12-16]. Hence, the understanding of such shape memory mechanisms is quite good. Detailed study and understanding of martensitic transformations in  $\text{Ni}_3\text{Sn}$  alloys is of interest, because  $\text{Ni}_3\text{Sn}$  martensite is one of the few martensites in nickel-based alloys that do not exhibit shape memory (SM) effects. Recent studies of  $\text{Ni}_3\text{Sn}$  alloys with added Cu have demonstrated that such alloys have a stable 2H phase at low temperature, which has the same structure as that of a martensite in a  $\text{Ni}_3\text{Sn}$  alloy[6]. In the literature, a new phase diagram was proposed[7]. After detailed investigation of the reported data, however, it was found that some phenomena could not be understood by the explanation given in the literature. Therefore, in the present case, we decided to study phase transformations in  $(\text{Ni,Cu})_3\text{Sn}$  alloys to obtain a correct phase diagram for the alloy system. A further reason for choice of this alloy system is that the phase transformations of ordered nickel-based alloys have not been studied as extensively as in Cu-base ordered alloys where martensitic transformations commonly manifest shape memory effect.

## 1.2 Martensitic Transformation in $DO_3$ Ordered Alloys

Most beta phases in noble-metal alloys, with a 3:2 electron-to-atom ratio,  $e/a$ , have an ordered bcc structure at high temperatures. The electron-to-atom ratio is defined as the average number of free electrons per atom. According to the electron theory of alloys, a bcc structure is considered to be stable at a value of  $e/a \sim 1.5$ , when a monovalent fcc noble metal (such as Au, Cu etc.) is alloyed with a bivalent metal (such as Zn, Cd etc.). As the number of free electrons increase with the addition of the bivalent metal, the density of available states decreases in the fcc structure than in a bcc structure. The peak in the density of state in the bcc phase occurs at about  $e/a = 1.48$ . Hence, the energy of the conduction electrons is lowered in the bcc structure at an electron-to-atom ratio of 1.5 compared with a fcc structure at the same  $e/a$  ratio [17].

Such a beta phase mostly has a fairly wide composition range of solubility at high temperatures. The stability of the beta phase decreases with decreasing temperature, resulting in a narrow range of solubility at lower temperatures. Thus, the beta phase usually decomposes below eutectoid temperatures of about  $700^\circ\text{C}$ . If, on the other hand, the beta phase is rapidly quenched to suppress the diffusion of atoms, the metastable beta-phase

transforms martensitically at a low temperature. Crystal structures of such transformation products are mostly close-packed layer structures. Because parent phase has an ordered structure, the martensite product phase inherits ordering since the transformation is diffusionless. Typical crystal structure of beta phases in noble-metal alloys manifest either an  $\text{Fe}_3\text{Al}(\text{DO}_3)$ -type superlattice (Figure 1.1) or a  $\text{CsCl}(\text{B2})$ -type superlattice. Both are called ordered bcc structures, although it should be noted that strictly speaking, the  $\text{DO}_3$  and B2 structures can be interpreted as fcc and simple cubic structures, respectively.

The  $\text{DO}_3$  structure is considered to be composed of two kinds of atom planes, A and B, that are alternately stacked parallel to the (110) close packed plane of the bcc structure (Figure 1.2). Martensitic structures are considered to be formed by a shear motion of atoms on the (110) planes of the bcc structure. It is possible to form six different types of close-packed layers by shear motions parallel to  $[\bar{1}\bar{1}0]$  on (110), although they are shifted relative to each other in the  $[\bar{1}\bar{1}0]$  directions. Such possible planes are shown in Figure 1.3, where the prime of A', B' and C' represents a change in atom arrangement of the A, B, and C planes, respectively, by  $b/2$  along the b-axis. For instance, the gamma-prime 2H structure (Figure 1.4) of  $\text{Ni}_3\text{Sn}$  has an  $\text{AB}'$  stacking order. For a 9R

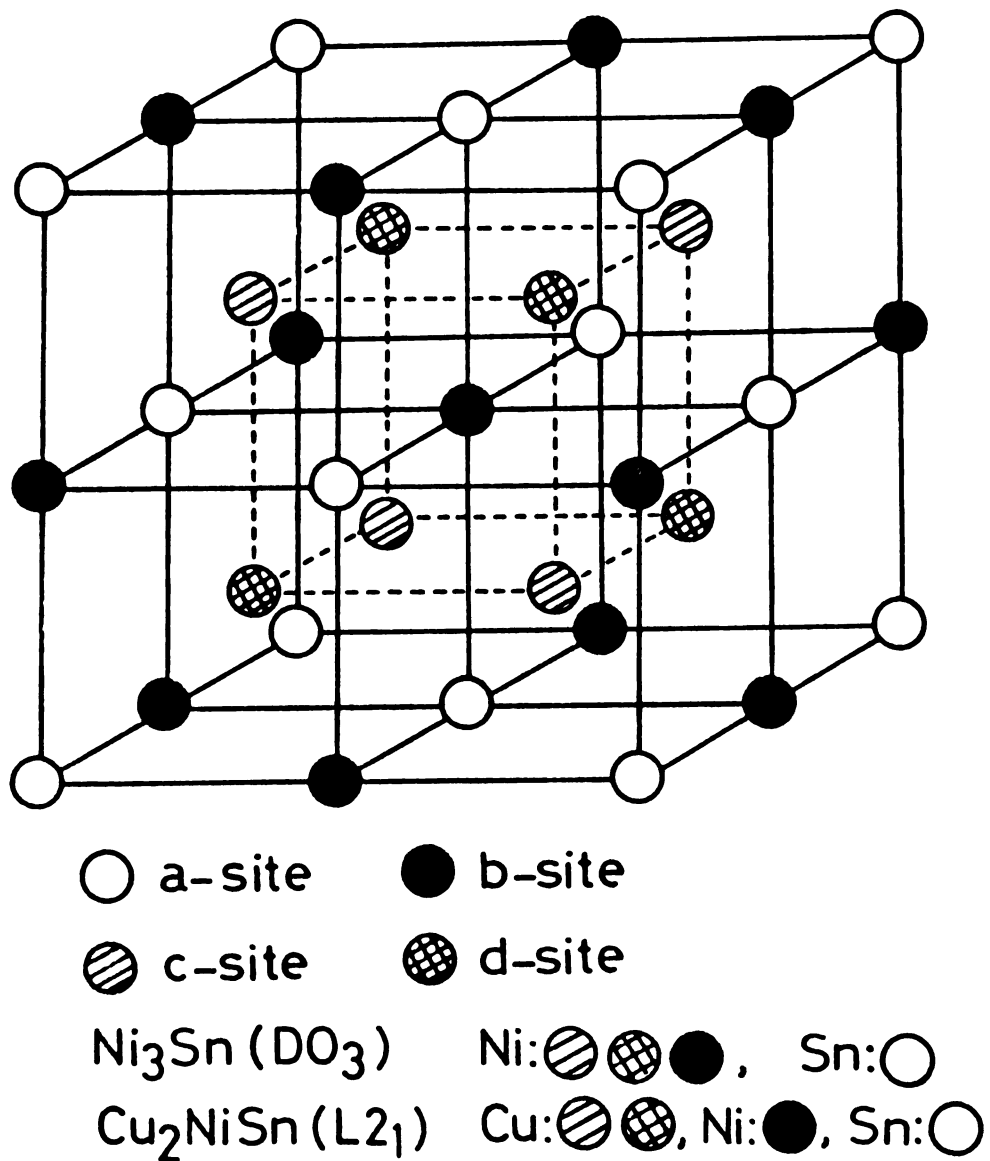


Figure 1.1 Unit cell of  $\text{D0}_3$ - and  $\text{L2}_1$ -type superlattices.

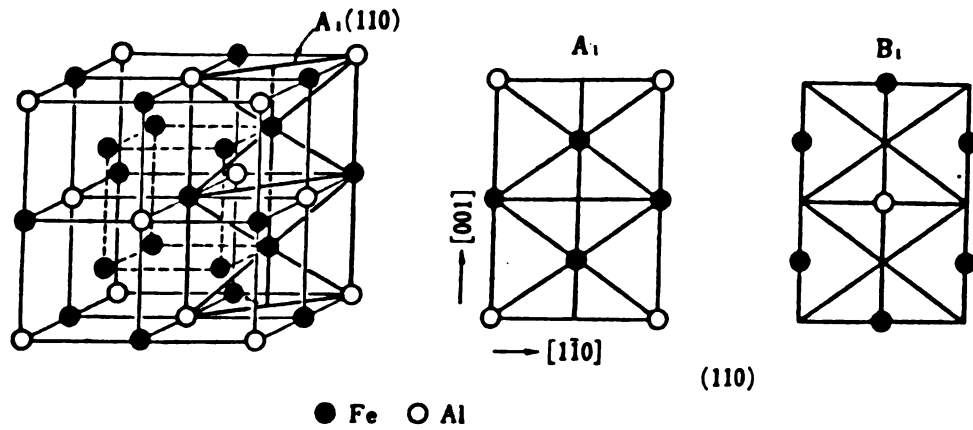


Figure 1.2 Two kinds of atomic layers, A and B, in (110) planes of  $DO_3$  structure.

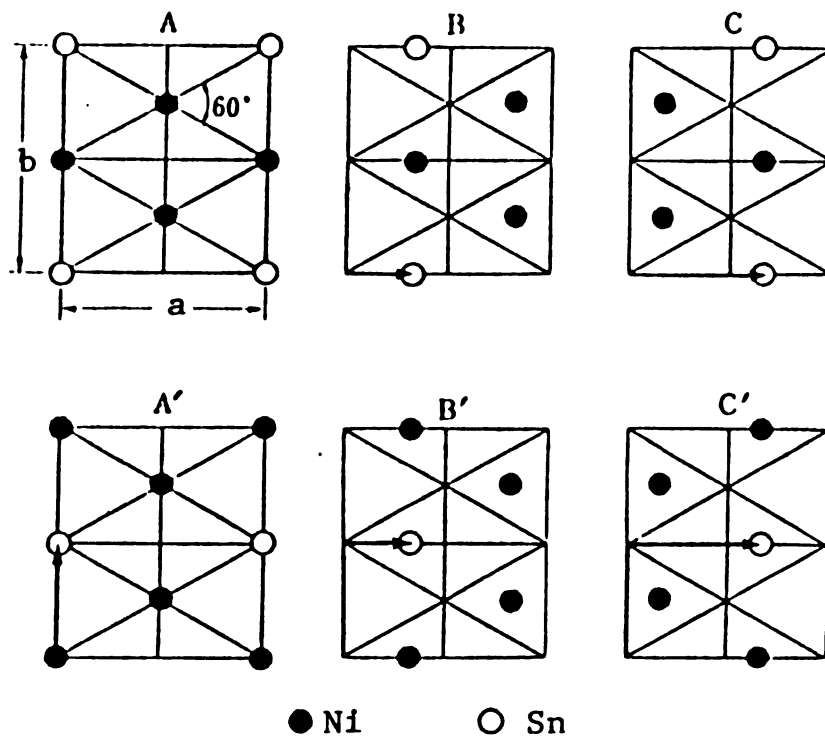


Figure 1.3 Six kinds of atomic layers in close-packed structures of martensite transformed from  $DO_3$ -type superlattice. The arrows indicate the displacement vector of each layer referred to layer A.

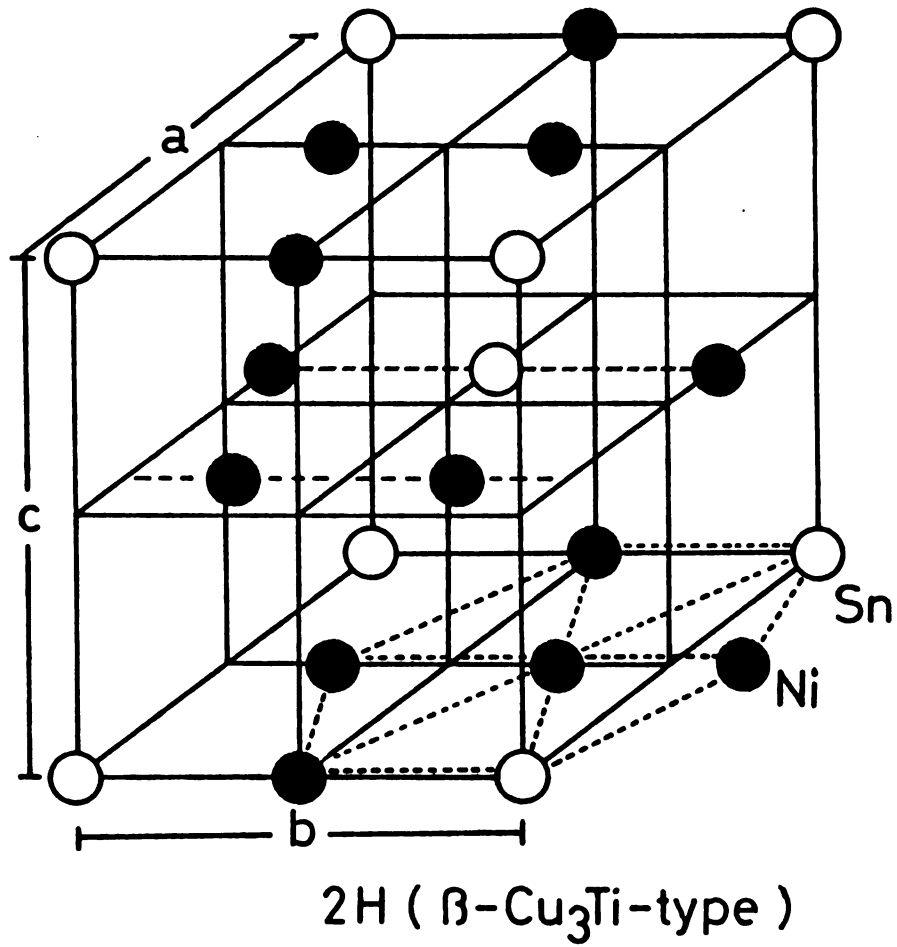


Figure 1.4 Unit cell of 2H (beta-Cu<sub>3</sub>Ti-type) superlattice.

structure (Figure 1.5), three layers constitute one subperiod. But, if atomic ordering is taken into consideration, the six layers AB'AC'BC' constitute one subperiod. Thus, the structure is called a 18R. If this subperiod stacking is taken as the unit cell, the resulting crystal type is a monoclinic structure. If nine layers AB'CB'CA'CA'B (so-called 9R) are taken as the unit cell, the crystal type is then an orthorhombic structure. The a- and b- axes in the orthorhombic coordinate system are shown in Figure 1.5; the c- axis is perpendicular to the close-packed plane.

Sato et al [18,19] explained the reason for the existence of the layer structures in terms of the electron theory of alloys. If stacking faults are introduced periodically into a crystal, the crystal has a long-period stacking order, resulting in the formation of a new Brillouin zone boundary. If the electron-to-atom ratio happens to be such that the Fermi surface is almost in contact with the newly formed Brillouin zone boundary, the gain energy of conduction electrons becomes greater than the increase in strain energy accompanied by the introduction of stacking faults at regular intervals. Thus, such long-period stacking structures become stable. This, however, needs atomic shuffling in addition to the shear motion of atoms.

Because energy differences among various kinds of

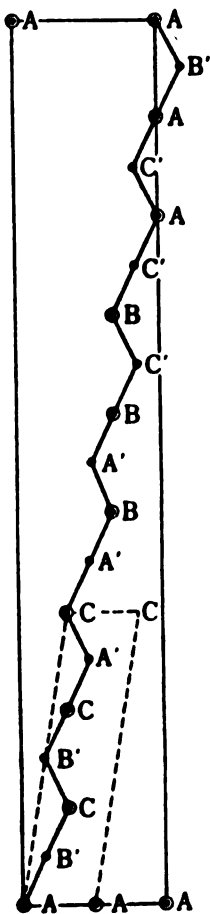


Figure 1.5 Stacking sequence of basal planes for a 9R structure.

long-period stacking structures are believed to be small, there are other factors, in addition to the alloy composition, that determine which long period stacking structure will be formed. In Cu-Al alloys, a martensite forms in the bulk specimen which has the 9R structure, while in a thin foil of the same alloy, another martensite having the 2H structure is formed[20]. In some other alloys, a mixture of two kinds of long-period stacking structure is formed. An example is the Au-Cd system, where the 2H and 9R structures are found in a lamellar form[19]. Factors to determine which long-range stacking structure should be present in an alloy have not yet been clarified.

### 1.3 Massive Transformations in Noble-Metal Alloys

In 1939, Greninger[21] found a patchy microstructure in a Cu-9.3 at% Al alloy with a fcc crystal structure. He designated this microstructure as "massive structure". This massive structure was obtained by quenching the alloy from a temperature range where the bcc high-temperature phase is stable. The massive structure showed equiaxial grains, and the grain boundaries were mostly straight with some irregularity but not oriented in specific directions. Essential differences between a precipitate and a massive structure are as follows; 1) the latter is not formed by

long-range diffusion of atoms and consists of the same alloy composition as the parent phase; that is, the massive transformation is a diffusionless one; 2) the precipitation takes place by long-ranged diffusion of atoms, resulting in compositional changes. More detailed descriptions of the massive transformation will be given below.

Since 1934, massive structures have been found in many other Cu alloys. These alloys are Cu-Ga, Cu-Zn, Cu-Zn-Ga and Cu-Ga-Ge alloys, all of which were studied by Masalski et al [22-24]. Saburi and Wayman [25] also found a massive structure in a Cu-23.8 at% Ga and studied the microstructure in detail by means of optical and transmission electron microscopy. They obtained the massive structure by quenching the beta phase of the alloy into warm water to avoid a eutectoid reaction at 610°C. It was found that this massive structure had the following morphological features: irregular or straight massive grain boundaries, a feathery structure, and a lamellar structure. The morphologies of the massive structure, thus, appear complex in form. The massive phase has a crystal structure and unique morphologies, different from those of a 18R martensite obtained by quenching specimens of the same alloy into ice water. An equilibrium phase diagram of the Cu-Ga system [23,26] is shown in Figure 1.6.

Masalski [22] also studied a massive structure of Cu-Ga alloys in detail and determined the crystal structure of

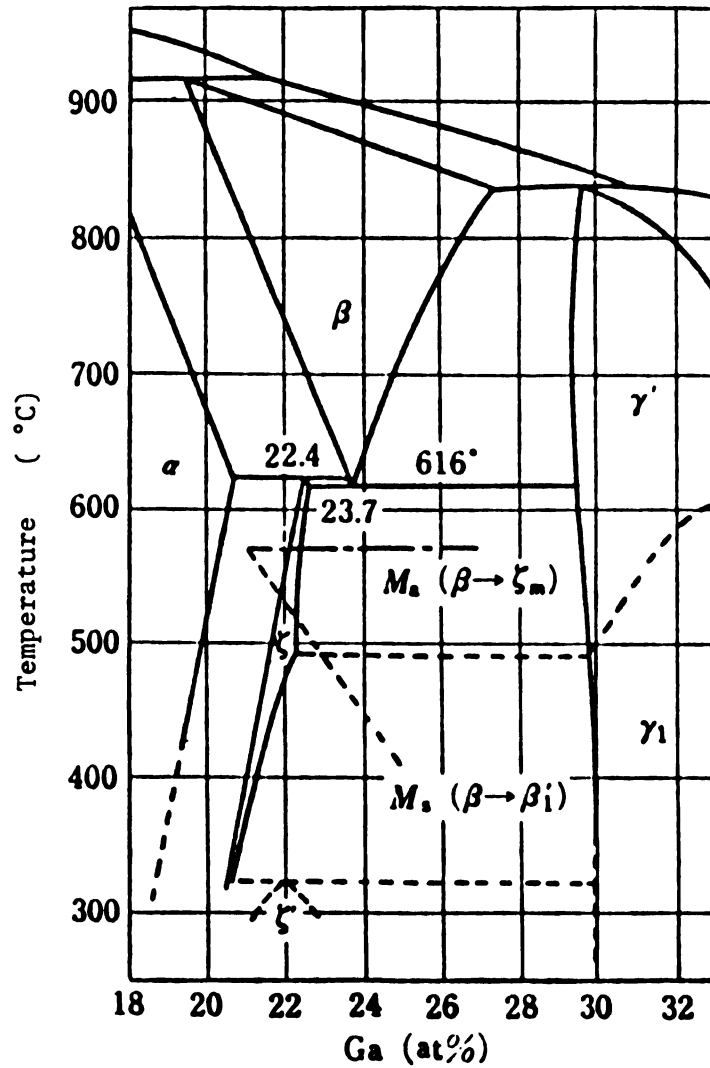


Figure 1.6 A portion of a phase diagram in the Cu-Ga system.

this phase (zeta-m phase) by X-ray diffraction. (The m herein indicates the phase formed by a massive transformation.) The structure determined of the zeta-m phase is a hcp structure, the same as the equilibrium zeta and zeta-prime phases. The lattice parameter of zeta-m phase increases linearly with Ga (Figure 1.7) [22]. This feature suggests that the zeta-m phase is not a decomposition product but a supersaturated solid solution of the zeta or zeta-prime phase. As can be seen from the phase diagram (Figure 1.7), a change in the lattice parameter,  $a$ , of composition of the zeta-m phase is the same as that for the beta parent phase. It is, hence, concluded that the massive transformation is governed by a diffusionless mechanism.

Significantly, the diffusionless character of this transformation is the same as that for martensitic transformations. However, there are some different features between massive and martensitic transformations. Kittl [26] studied the effect of quenching rates on  $M_a$  temperature (temperature at which a massive transformation starts to take place). He found that the  $M_a$  temperature of Cu-Ga alloys did not show any considerable change when the quenching rate was changed between 10 and 2500°C/sec. It should be noted that the  $M_a$  temperature was higher than the  $M_s$  temperature (at which martensitic transformations start to take place) of the

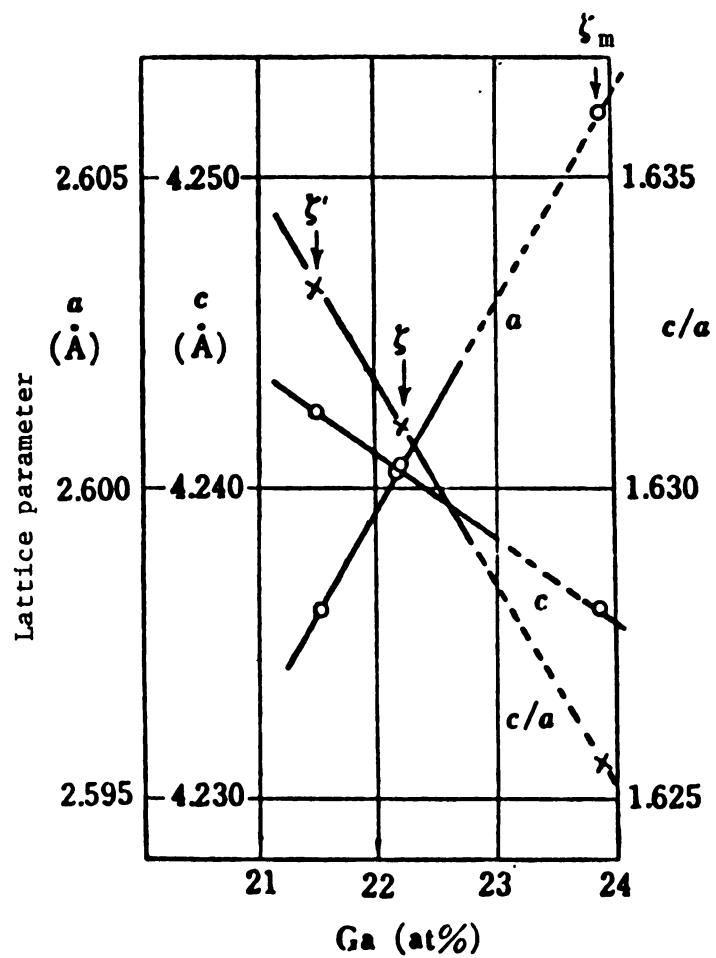


Figure 1.7 Lattice parameters of  $\zeta$ ,  $\zeta'$ , and  $\zeta_m$  phases in the Cu-Ga system.

alloys.

Kittl [26] also found another peculiar characteristic in the zeta-m phase. That is, there is no unique orientation relationship between the beta matrix phase and the zeta-m phase. Grains of the zeta-m phase are often seen to have grown across grain boundaries of the parent phase[23]. Such phenomena are not observed in the case of martensitic transformations. In this case, specific orientation relationships are present and no martensites can grow across grain boundaries of their parent phase.

Transmission electron microscopy and electron diffraction techniques showed that there were numerous internal faults in the zeta-m phase. These internal faults are parallel to the (0001) basal plane of the zeta-m(hcp) phase. It is interesting that the number of faults is less in the zeta-m phase than in the martensite. When quenching rate is very low, only a few faults are formed in the zeta-m phase. This lesser number of internal faults in the massive structure suggests that the massive transformation occurs with some sort of diffusion of atoms. From observations of microstructural features and changes in lattice parameters, however, this diffusion appears to be short-range diffusion, rather than long-range diffusion.

#### 1.4 The Ni<sub>3</sub>Sn System

An equilibrium phase diagram of the binary Ni-Sn system was shown in Figure 1.8 [27]. The Ni<sub>3</sub>Sn alloy has a DO<sub>19</sub> ordered hexagonal structure at low temperatures and a DO<sub>3</sub> ordered structure at high temperatures. Because a phase transformation to the DO<sub>19</sub> phase was not clear, Nial [28] studied the crystal structure of the DO<sub>3</sub> high temperature phase. He reported that X-ray data obtained from a quenched powder specimen showed a disordered hcp structure, and concluded that a transformation to the DO<sub>19</sub> phase was an order-disorder one. This conclusion was not consistent with X-ray data of the high temperature phase reported by Schubert et al [29]. They used high temperature X-ray equipment and determined the crystal structure to be a DO<sub>3</sub> structure. The DO<sub>3</sub> structure at high temperature was strongly supported by a study carried out by Pak et al [6].

Pak et al [6] studied phase transformations of the high temperature phase by detailed microstructural observations and identification of phases present in specimens. The specimens used were quenched from 1050°C (a temperature region of the DO<sub>3</sub> phase) at several different cooling rates. Methods of investigation included metallography, electron microscopy, and electron and X-ray diffraction techniques. The reported results are

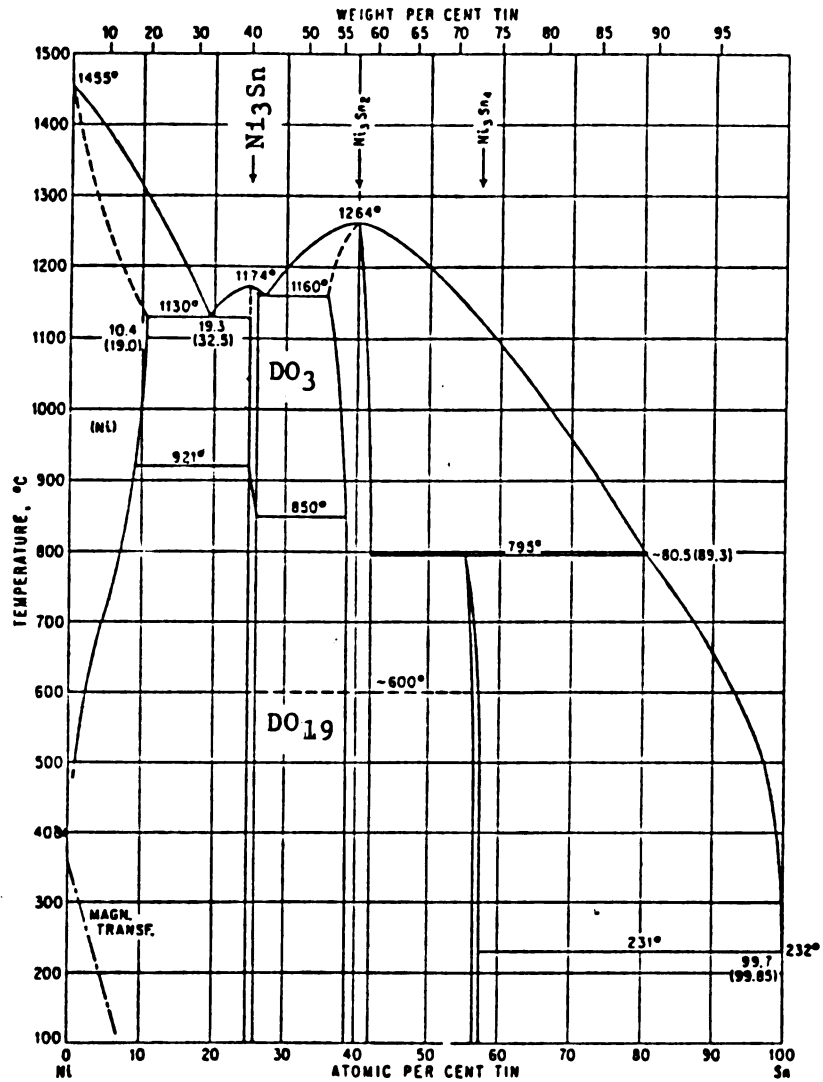


Figure 1.8 Phase diagram of Ni-Sn system.

described as follows.

A massive transformation was found to have taken place by quenching from 1050° to 0°C at cooling rates of 10°C/hr, 40°C/sec and 200°C/sec. Grains of the massive phase crossed original grain boundaries of the parent phase during their growth, similar to observations made of other massive phases. The crystal structure of the massive phase in the Ni<sub>3</sub>Sn was a DO<sub>19</sub> ordered hexagonal structure, the same as that for the stable phase at low temperature. Microstructures of the massive phase are different from those of the stable low-temperature phase, although both the phases have the same crystal structure. The massive phase contained planar faults parallel both on the basal (0001) plane and on the prism (10 $\bar{1}$ 0) plane, while the stable phase did not contain such planar faults but contained a few grown-in dislocations.

On the other hand, when the high temperature DO<sub>3</sub> phase was quenched at a rate of 200°/sec or higher, very fine acicular structures were formed. These structures clearly showed surface relief, and thus it was concluded that they were martensites. The crystal structure of the acicular martensite was determined to be a 2H ordered orthorhombic structure (beta-Cu<sub>3</sub>Ti-type), which may be called a deformed hcp structure. Pak et al [6] named this martensite phase the gamma-prime phase. This gamma-prime martensite contains (121)<sub>2H</sub> internal twins, which provide

the lattice invariant strain. By taking into account atomic arrangements of the (0001) massive plane and the (001) martensite plane, and by also taking into account  $\{10\bar{1}0\}$  planar faults in the massive phase, a relationship between the  $DO_{19}$  massive phase and the 2H martensite phase can be determined. As seen in Figure 1.9, which shows atomic arrangements for these two phases, it is possible to produce planar faults by applying an  $a/2 \langle 1\bar{2}10 \rangle$  shear on every other  $\{10\bar{1}0\}$  plane [6]. Hence, planar faults observed in the massive structure are most probably thin crystals of the 2H martensite phase. Until recently, because of a difficulty of retaining the parent phase of  $DO_3$  structure at room temperature, no orientation relationship between the 2H martensite and the  $DO_3$  parent phase was reported.

Recently, Chang [30] proposed a new method of determining the orientation of the parent phase and the habit plane normals of a plate-shaped product phase, without the need for retaining the parent phase at observation temperatures. This method only requires the sufficient number of traces formed by the intersection of product phase variants with a surface of a specimen. Such a surface is assumed to be the surface of the parent phase. Pak et al [31], more recently, developed the model proposed by Chang [30] and applied their model to the martensite in the  $Ni_3Sn$  alloy.

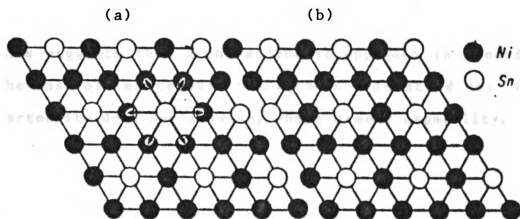


Figure 1.9 Atomic arrangements in the (0001) plane of DO<sub>19</sub> structure (a) and in the (001) plane of 2H structure (b).

The habit plane of a martensite in  $\text{Ni}_3\text{Sn}$  was determined to be  $\{133\}$ . It is to be mentioned that a 2H-type martensite in a Cu-Al-Ni alloy, formed from a  $\text{DO}_3$ -type structure of the parent phase, has a shape-memory effect and the martensite, has the same habit plane as the martensite in the  $\text{Ni}_3\text{Sn}$  alloy. In addition, the martensite in the Cu-Al-Ni and  $\text{Ni}_3\text{Sn}$  alloys both have  $\{121\}$  internal twins. It is interesting, however, that the latter alloy does not show any shape-memory effect. This suggests that a thermodynamic approach is needed in the case of martensite in  $\text{Ni}_3\text{Sn}$  to understand why this martensite does not show any shape memory capability.

## 1.5 The $(\text{Ni,Cu})_3\text{Sn}$ System

As seen in the phase diagram for the Ni-Sn system (Figure 1.8) the high temperature  $\text{DO}_3$  phase is transformed at around  $900^\circ\text{C}$ . Since this transition temperature is high Murakami et al [7-9] attempted to make it lower by substituting copper atoms for nickel atoms. They studied phase changes in several Ni-xCu-25Sn alloys (x=atomic percent) by means of X-ray diffraction, differential thermal analysis, and optical and electron microscopy. A new phase diagram of the ternary Ni-xCu-25Sn system (Figure 1.10), was proposed based on data obtained by Murakami et al [7-9]. It was reported that a phase transformation from a  $\text{DO}_3$  structure to a 2H structure and that from the 2H structure to a  $\text{DO}_{19}$  structure were observed by means of electron microscopy in the Ni-4Cu-25Sn alloy.

As seen in Figure 1.10, three phases with  $\text{DO}_3$ , 2H and  $\text{DO}_{19}$  structures were stable at room temperature, while in the binary Ni-Sn system the  $\text{DO}_{19}$  hexagonal phase is the only phase at room temperature. In a range of copper contents up to 6.5 at.%, two transformations were found. One is a martensitic transformation from the  $\text{DO}_3$  phase to the 2H phase, taking place at high temperature upon rapid quenching, and the other is a massive transformation from the  $\text{DO}_3$  phase to the  $\text{DO}_{19}$  phase, taking place upon slow

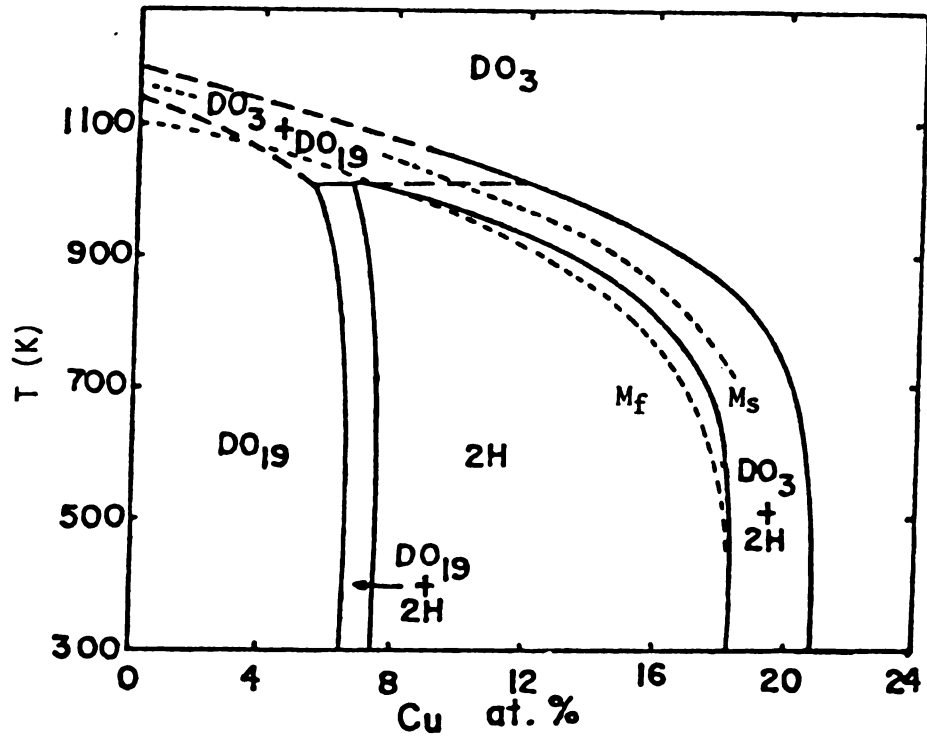


Figure 1.10 Phase diagram of Ni-xCu-25Sn alloys.

cooling. In a range of copper contents from 7.5 to 18 at%, the  $DO_3$  phase undergoes a martensitic transformation to a phase with the 2H structure upon rapid quenching.

Murakami et al [8] also reported that for this range, a low-temperature 2H phase was massively transformed upon furnace cooling. Microstructural features of the massive 2H phase are different from those of the martensite 2H phase. Stacking faults and other planar defects are considerably less abundant in the massive phase than in the martensite phase. By taking structural observations into account, it was speculated that if the cooling rate becomes slower, the morphology could gradually change from a martensite-type structure to a massive-type structure by the migration of interfaces upon cooling.

The following point is important and thus should be emphasized. According to the phase diagram proposed by Murakami et al [7-9], the  $DO_3$  parent phase and the massive and/or martensite 2H phase should be retained at room temperature in a range of copper contents between 18 and 21 at%. Thus, one can expect that some crystallographic information, such as orientation relationships between the martensite and the parent  $DO_3$  phase, or those between the massive and the parent phase could be obtained. No such relationships have yet been observed directly both for  $Ni_3Sn$  and for the  $(Ni,Cu)_3Sn$  alloys.

## 2 OUTLINE OF THE PRESENT WORK

As pointed out in the previous section, if the phase diagram of the Ni-xCu-25Sn proposed by Murakami et al is correct, then the higher temperature  $DO_3$  phase could be retained in the range of copper contents, x, between 18 and 21 at%. Hence, the orientation relationship between the  $DO_3$  parent and the product phases should be readily clarified for both the binary and ternary Ni-xCu-25Sn alloys. Attempts to produce two-phase specimens were made. Surprisingly, however, no  $DO_3$  phase could be obtained by changing both cooling rates and Cu content. This indicates that the phase diagram proposed by Murakami et al [7-9] is incorrect. The present work, thus, primarily focuses on clarifying phase transformations which occur in ternary Ni-xCu-25Sn alloys. As a further result of the present study, a new equilibrium phase diagram is proposed. Various aspects of this investigation are itemized as follows:

(1) X-ray diffraction experiments were conducted to reexamine the phase diagram of the Ni-xCu-25Sn alloys (x ranging from 5 to 22). Since some uncertainties remained in the range of copper contents between 10 and 20%, special attention was paid to phase changes occurring in this composition range. Crystal structures were determined by a Debye-Scherrer method.

(2) As mentioned in the previous section, the 2H structure in the  $(\text{Ni,Cu})_3\text{Sn}$  alloys was obtained by furnace cooling, and was reported to be a stable, equilibrium phase. It was also reported that this stable phase was only present in the range of copper compositions from 7.5 to 18 at% Cu. In the present study, however, it was found that there were several X-ray diffraction peaks that were obtained in furnace-cooled specimens. These peaks could not be indexed by any familiar structures in this alloy system, such as 2H,  $\text{DO}_{19}$ , and  $\text{DO}_3$  structures. These results suggested the presence of a previously unrecognized new phase. Therefore, careful, detailed microscope observations were made in order to confirm the presence of a new phase in this region.

(3) Transmission electron microscopy and electron diffraction analysis were employed extensively for identification and characterization of the new phase which was found.

(4) Based upon results obtained through electron diffraction analyses and electron microscopy, a new phase diagram is proposed. Results obtained by differential thermal analysis were incorporated into this phase diagram.

(5) Detailed microstructural observation of phases formed under various conditions were made.

### 3 EXPERIMENTAL PROCEDURES

#### 3.1 Preparation and Heat Treatment of Alloys

Several ternary alloys were prepared from pure nickel (99.999% purity), electrolytic copper (99.99%) and pure tin (99.999%). These pure metals were encapsulated in quartz tubes (18mm diameter) after evacuation to about  $10^{-3}$ MPa. Encapsulated pure metals were then alloyed in a resistance furnace and stirred vigorously several times to produce alloys as homogeneous as possible. Weight loss was less than 0.5% after alloying. Out of several alloys produced, the three alloys, Ni-14Cu-25Sn, Ni-17.5Cu-25Sn, and Ni-20Cu-25Sn, were extensively investigated.

The alloy ingots were again encapsulated in evacuated quartz tubes and homogenized for two days at 1000°C, and subsequently air-cooled. Because all the alloys produced were brittle, none could be rolled. The ingots were, therefore, sliced with a diamond blade and slices (about 0.5mm thickness) were then encapsulated in evacuated quartz tubes to anneal them at 1000°C for 2 hr. Then various heat treatments were performed. The heat treatments employed are listed in Figure 3.1, and their purposes are given as follows:

[1] After annealing for 2 hr at 1000°C, some specimens were furnace cooled to investigate crystal structures and

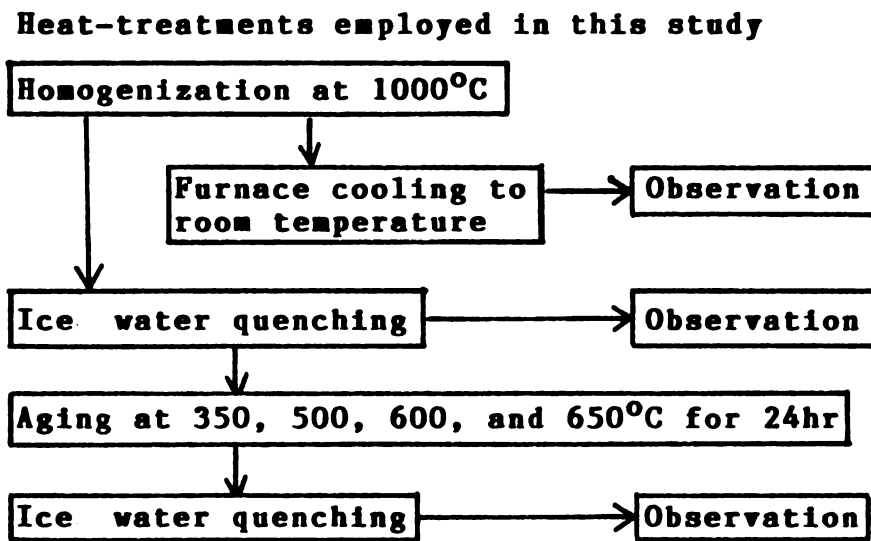


Figure 3.1 Flow chart of heat treatments employed.

microstructures of phases present.

[2] Annealing for 1 hr at 1000°C , followed by quenching into ice water (the quartz capsules were crushed during quenching), was made for the observation of the DO<sub>3</sub> and martensite phases.

[3] Some quenched specimens (of Ni-20Cu-25Sn alloy) were aged at 350, 500, 600, and 650°C for 24 hr to determine both phase boundaries and transformation temperatures.

### 3.2 Optical Microscopy, X-ray Diffraction Analysis, and Scanning and Transmission Electron Microscopy

Thin foils for transmission electron microscopy were made with a twin-jet Fishione electro-polisher and a conventional polisher. The polishing solution was a mixture of 75vol% ethanol and 25vol% perchloric acid, and polishing was done at -60°C. Transmission electron microscope observations were made with Hitachi H-800 and HU-200F electron microscopes, both of which were operated at 200keV.

Powder samples were prepared for X-ray Debye-Scherrer and diffractometer methods. The powder samples were encapsulated in a way similar to that mentioned above and then heat-treated. In this case, the capsules were not crushed. Cu radiation was used for all X-ray experiments.

Specimens for optical microscope observation were

electro-polished following mechanical polishing. The electro-polishing solution used was the same as that for transmission electron microscopy. After electro-polishing, the specimens were kept for about 1 min in the same solution for slight etching. For optical microscopy, a Nikon microscope with a Nomarski-type interference capability was employed. For observation of surface relief for fine structures formed during furnace cooling, a Hitachi HHS-2R scanning electron microscope was used. This electron microscope was operated at 30 keV.

### 3.3 Differential Thermal Analysis

In order to obtain the temperature of phase transition, a DuPont Thermal Analyzer (model 990) was used. This analyzer was designed to provide two kinds of data which are obtainable by differential scanning calorimeter (DSC) and differential thermal analysis (DTA) methods. In the present study, we used data obtained by the latter method because higher temperatures could be achieved in this mode. In the DTA method, the transition temperature is given by an intersection of a pair of the tangents to concave or convex DTA response curves corresponding to an exothermic or an endothermic reaction, respectively.

In each experiment, a specimen of approximately 70 mg was used and a heating rate of  $10^{\circ}\text{C}/\text{min}$  was employed in all experiments. During the experiments, dry argon gas was passed through the furnace tube of the DTA to maintain an inert atmosphere. Alloys prepared in this study were ones containing Cu contents of 14, 17.5, and 20 at%, and these specimens were quenched from  $1000^{\circ}\text{C}$  to ice water prior to DTA experiments.

## 4 EXPERIMENTAL RESULTS AND DISCUSSIONS

### 4.1 Optical and Scanning Electron Microscopy

Surface observations of microstructures in the Ni-14Cu-25Sn alloy were carried out by means of optical microscopy and scanning electron microscopy. Figure 4.1 shows a typical micrograph of a Ni-14Cu-25Sn specimen, which was annealed at 1000°C to produce the high temperature beta ( $\text{DO}_3$ ) phase and then slowly cooled in an electric resistance furnace. From the morphology seen in Figure 4.1, it is obvious that at least two phases were co-existing under the above-mentioned conditions. The cooling rate in this case was estimated to be approximately 20°C/min in the temperature range from 1000°C to 400°C. Thus, all phases obtained are considered stable.

As seen in the photomicrograph in Figure 4.1, the most abundant phase has a taper-ended, rod-shape microstructure. This phase appears as bright bands in the figure. The width of these bands varies from 10 to 30  $\mu\text{m}$ . Figure 4.2 shows a similar structure obtained from another area of the same specimen which reveals more details about this rod-shaped structure. It is seen to consist of fine microstructures, which bear resemblance to the midribs of a ferrous martensite. The rod-shaped phase was identified as a 2H ordered structure by X-ray and

**Figure 4.1** Microstructure of a Ni-14Cu-25Sn alloy,  
furnace-cooled from 1000°C to room  
temperature.

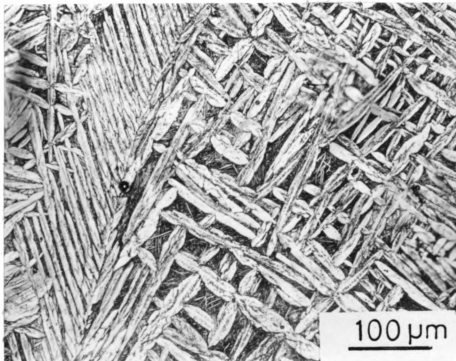
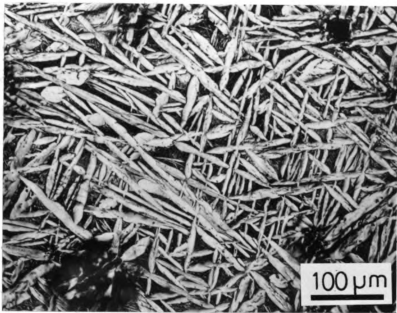


Figure 4.2 Microstructure of a Ni-14Cu-25Sn alloy,  
furnace-cooled from 1000°C to room  
temperature.



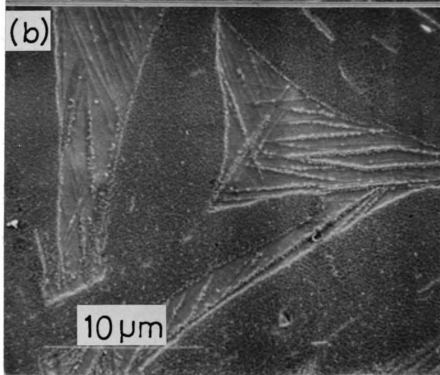
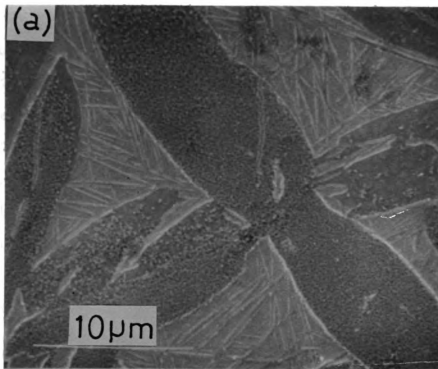
transmission electron diffraction analyses, as will be described below.

The less abundant phase is seen between bands of the afore-mentioned rod-shaped phase. It appears as dark areas in figures 4.1 and 4.2. Upon close examination by scanning electron microscopy, it was found that the dark areas are comprised of numerous, very fine acicular structures. Figures 4.3(a) and (b) are scanning electron micrographs of a specimen which was electro-polished immediately prior to observation. From these photos, it is seen that the acicular structures (which are surrounded by the 2H, rod-shaped structures) appear to have specific orientations to the parent phase. Taking this alignment of such acicular structures into account, one can conclude that they nucleated in the parent phase and grew in such a way as to have a specific orientation relationship with the original matrix of the  $DO_3$  phase.

Determination of this orientation relationship would be of interest. However, in this study this was difficult because no parent  $DO_3$  phase could be retained by furnace cooling. An attempt was made to apply a method developed by Pak et al [31] which was used for identification of the habit plane of plate-like microstructures. Unfortunately, the method was found not to be applicable in this case, because there were multi-phases in one grain.

Similar acicular structures were observed in two

Figure 4.3 Scanning electron micrographs of a Ni-14Cu-25Sn alloy, furnace-cooled from 1000°C.



other alloys, Ni-17.5Cu-25Sn and Ni-20Cu-25Sn. Figure 4.4 shows a typical example of acicular structures that were obtained in a Ni-17.5Cu-25Sn specimen furnace-cooled from 1000°C to room temperature. Another example is shown in Figure 4.5, which was obtained from a furnace-cooled Ni-20Cu-25Sn specimen. In these figures, no rod-shaped structures were noted by optical microscopy. However, it is obvious that two phases are present in both cases. One phase appears to have a wider and longer plate shape, while the other has a narrower and shorter plate shape. To obtain further details about these phases, X-ray diffraction experiments were carried out for the previously mentioned three alloys; the results are discussed in the following section.

**Figure 4.4** Microstructure of a Ni-17.5Cu-25Sn alloy,  
furnace-cooled from 1000°C.

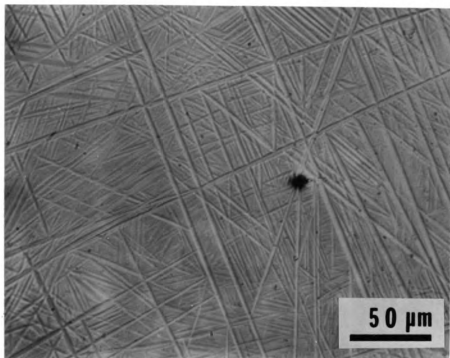
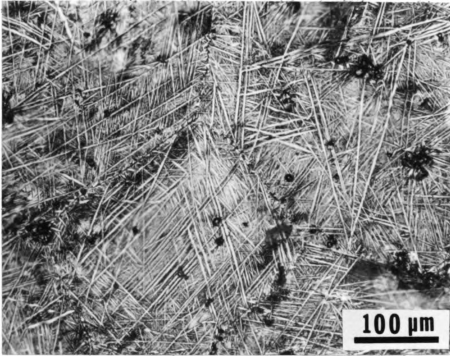


Figure 4.5 Microstructure of a Ni-20Cu-25Sn alloy,  
furnace-cooled from 1000°C.



## 4.2 Results of Diffractometer and Debye-Scherrer Methods

Figure 4.6 shows the results of an X-ray diffractometer examination of a powder specimen of the Ni-17.5Cu-25Sn alloy, furnace-cooled from 1000 °C to room temperature. Because an orthorhombic 2H stacking ordered structure was reported to exist both in quenched specimen of the Ni<sub>3</sub>Sn alloy [6] and the Ni-xCu-25Sn (x=4-8) alloys [7-9], we first tried to index reflection peaks obtained by assigning the 2H structure. As shown in Figure 4.6, most of the peaks could be indexed by reflection indices of the 2H structure. The angles and d-spacings measured allowed determination of lattice parameters of the 2H structure as a=4.495, b=5.380, and c=4.285Å. These values are in agreement with those reported by Pak et al [6] and Murakami et al [7,9].

The theoretical intensities of reflections were also calculated and listed in Table 4.1. From this table, it can be found that there are no strong peaks between (121)<sub>2H</sub> and (002)<sub>2H</sub>. Thus, peaks 5 and 6 in Figure 4.6 could not be indexed by any reflection indices of the 2H structure, indicating the presence of another phase. This is inconsistent with the phase diagram proposed by Murakami et al [7]. One of these unidentified peaks probably can be indexed by a reflection index of a DO<sub>3</sub>

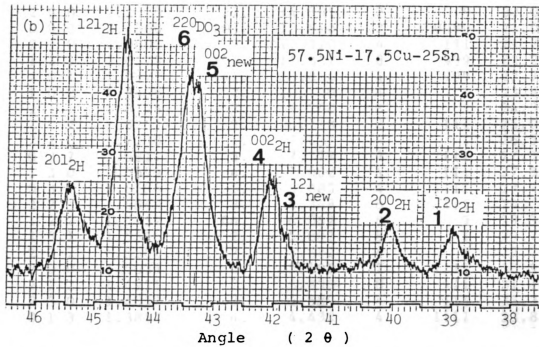


Figure 4.6 Partial diffractometer pattern of a furnace-cooled Ni-17.5Cu-25Sn alloy.

Table 4.1 Angles and intensities of reflection peaks for a 2H-orthorhombic structure of a furnace-cooled Ni-14Cu-25Sn alloy. Lattice parameters used for theoretical calculation:  $a=4.510$ ,  $b=5.393$ ,  $c=4.300\text{\AA}$ ; Cu-k alpha:  $1.544390\text{\AA}$ ; Debye-Scherrer method used.

H	K	L	D-SPAC	INTEN	L-P	MULTI	SF	THETA
1	0	0	4.5100	1.	65.304	2	1	9.86
1	1	0	3.4597	8.	37.286	4	111	12.90
0	1	1	3.3621	11.	35.062	4	1111	13.28
1	0	1	3.1122	7.	29.660	4	111	14.37
0	2	0	2.6965	18.	21.622	8	1111	16.64
1	1	1	2.6955	5.	21.604	8	1	16.65
1	2	0	2.3144	56.	15.287	4	9	19.49
2	0	0	2.2550	27.	14.395	2	9	20.03
0	0	2	2.1500	103.	12.880	2	9999	21.05
2	1	0	2.0805	5.	11.920	4	111	21.79
1	2	1	2.0379	290.	11.351	8	999	22.27
2	0	1	1.9970	141.	10.816	4	999	22.75
1	0	2	1.9408	2.	10.100	4	1	23.45
2	1	1	1.8728	3.	9.268	8	1	24.35
1	1	2	1.8261	9.	8.718	8	111	25.02
2	2	0	1.7298	1.	7.637	4	1	26.51
0	2	2	1.6811	5.	7.118	4	1111	27.35
1	3	0	1.6699	4.	7.002	4	111	27.54
0	3	1	1.6586	5.	6.885	4	1111	27.75
2	2	1	1.6048	8.	6.348	8	111	28.76
1	2	2	1.5752	66.	6.062	8	9	29.36
1	3	1	1.5566	2.	5.887	8	1	29.74
2	0	2	1.5561	32.	5.882	4	9	29.75
3	0	0	1.5033	2.	5.403	2	1111	30.91
2	1	2	1.4951	7.	5.330	8	111	31.10
2	3	0	1.4057	3.	4.589	4	111	33.32
0	1	3	1.3852	4.	4.432	4	1111	33.88
3	1	1	1.3724	8.	4.335	8	1111	34.24
1	0	3	1.3660	3.	4.288	4	111	34.42
0	4	0	1.3483	208.	4.159	8	9999	34.94
2	2	2	1.3478	2.	4.155	8	1	34.96
2	3	1	1.3361	2.	4.073	8	1	35.31
1	1	3	1.3242	2.	3.990	8	1	35.67
1	3	2	1.3188	6.	3.954	8	111	35.84
3	2	0	1.3131	100.	3.915	4	9999	36.02
1	4	0	1.2918	1.	3.775	4	1	36.71
1	4	1	1.2371	5.	3.446	8	111	38.62
3	0	2	1.2320	3.	3.417	4	1111	38.81
1	2	3	1.2186	137.	3.344	8	999	39.32
2	0	3	1.2097	68.	3.297	4	999	39.67
2	1	3	1.1803	2.	3.153	8	1	40.86

H	K	L	D-SPAC	INTEN	L-P	MULTI	SF	THETA
2	3	2	1.1765	5.	3.136	8	111	41.02
2	4	0	1.1572	22.	3.051	4	9	41.86
0	4	2	1.1422	88.	2.991	4	9999	42.53
4	0	0	1.1275	11.	2.937	2	9	43.23
0	3	3	1.1207	3.	2.914	4	1111	43.55
3	2	2	1.1206	174.	2.913	8	9999	43.56
2	4	1	1.1174	130.	2.903	8	999	43.71
3	3	1	1.1139	7.	2.891	8	1111	43.89
1	4	2	1.1073	2.	2.871	8	1	44.22
2	2	3	1.1037	5.	2.860	8	111	44.40
4	1	0	1.1036	2.	2.860	4	111	44.40
4	0	1	1.0906	65.	2.825	4	999	45.07
1	3	3	1.0876	2.	2.817	8	1	45.23
0	0	4	1.0750	43.	2.789	2	9999	45.92
4	1	1	1.0690	2.	2.777	8	1	46.25
1	5	0	1.0490	3.	2.746	4	111	47.40
0	5	1	1.0462	3.	2.742	4	1111	47.57
1	0	4	1.0457	1.	2.742	4	1	47.60
4	2	0	1.0402	1.	2.737	4	1	47.93
1	1	4	1.0266	5.	2.729	8	111	48.78
1	5	1	1.0191	2.	2.728	8	1	49.26
2	4	2	1.0190	45.	2.728	8	9	49.27
3	1	3	1.0187	7.	2.728	8	1111	49.29
4	2	1	1.0111	5.	2.730	8	111	49.80
3	4	0	1.0037	4.	2.734	4	1111	50.29
2	3	3	1.0036	2.	2.734	8	1	50.30
0	2	4	0.9986	4.	2.739	4	1111	50.65
4	0	2	0.9985	23.	2.739	4	9	50.65
4	1	2	0.9818	6.	2.765	8	111	51.86
1	2	4	0.9750	48.	2.781	8	9	52.38
2	5	0	0.9730	3.	2.786	4	111	52.52
2	0	4	0.9704	24.	2.793	4	9	52.73
1	4	3	0.9596	6.	2.828	8	111	53.58
4	3	0	0.9552	3.	2.845	4	111	53.94
2	1	4	0.9550	6.	2.845	8	111	53.95
2	5	1	0.9490	2.	2.871	8	1	54.46
1	5	2	0.9428	6.	2.902	8	111	54.99
4	2	2	0.9364	2.	2.937	8	1	55.55
4	3	1	0.9324	2.	2.961	8	1	55.91
2	2	4	0.9131	2.	3.106	8	1	57.75
3	4	2	0.9095	10.	3.138	8	1111	58.11
1	3	4	0.9039	7.	3.193	8	111	58.68
5	0	0	0.9020	1.	3.213	2	1	58.88
2	4	3	0.9004	184.	3.230	8	999	59.05
0	6	0	0.8988	10.	3.247	8	1111	59.22
3	3	3	0.8985	10.	3.251	8	1111	59.25
5	1	0	0.8896	4.	3.359	4	111	60.23
2	5	2	0.8865	8.	3.402	8	111	60.59
4	0	3	0.8862	99.	3.406	4	999	60.62

H	K	L	D-SPAC	INTEN	L-P	MULTI	SF	THETA
5	0	1	0.8828	4.	3.455	4	111	61.01
1	6	0	0.8815	34.	3.475	4	9	61.16
4	1	3	0.8745	3.	3.589	8	1	62.01
3	0	4	0.8744	6.	3.589	4	1111	62.02
4	3	2	0.8729	9.	3.616	8	111	62.21
5	1	1	0.8712	3.	3.646	8	1	62.42
4	4	0	0.8649	38.	3.768	4	9	63.23
1	6	1	0.8635	228.	3.797	8	999	63.41
0	5	3	0.8618	6.	3.834	4	1111	63.64
3	5	1	0.8587	13.	3.904	8	1111	64.06
5	2	0	0.8554	40.	3.984	4	9	64.52
2	3	4	0.8539	10.	4.022	8	111	64.73
0	1	5	0.8493	7.	4.147	4	1111	65.40
4	4	1	0.8479	257.	4.185	8	999	65.60
1	5	3	0.8465	4.	4.227	8	1	65.81
1	0	5	0.8448	5.	4.280	4	111	66.08
4	2	3	0.8419	11.	4.374	8	111	66.52
0	4	4	0.8405	183.	4.420	4	9999	66.74
5	2	1	0.8390	278.	4.475	8	999	66.99
2	6	0	0.8349	2.	4.626	4	1	67.64
1	1	5	0.8346	4.	4.640	8	1	67.70
3	2	4	0.8318	398.	4.756	8	9999	68.18
5	0	2	0.8318	2.	4.758	4	1	68.18
0	6	2	0.8293	9.	4.868	4	1111	68.62
1	4	4	0.8263	4.	5.011	8	1	69.15
5	1	2	0.8220	14.	5.237	8	111	69.94
2	6	1	0.8196	15.	5.379	8	111	70.41
1	6	2	0.8156	122.	5.644	8	9	71.22
5	3	0	0.8062	9.	6.436	4	111	73.30
1	2	5	0.8061	425.	6.443	8	999	73.31
2	5	3	0.8050	6.	6.557	8	1	73.58
2	0	5	0.8035	223.	6.723	4	999	73.94
4	4	2	0.8024	152.	6.856	8	9	74.22
4	3	3	0.7948	8.	7.991	8	1	76.29
5	2	2	0.7948	181.	7.998	8	9	76.30
2	1	5	0.7948	8.	8.006	8	1	76.31
5	3	1	0.7924	8.	8.489	8	1	77.03
2	4	4	0.7876	225.	9.786	8	9	78.65
4	5	0	0.7794	22.	14.477	4	111	82.20
2	6	2	0.7783	16.	15.729	8	1	82.81
4	0	4	0.7780	191.	16.109	4	9	82.97
0	3	5	0.7758	43.	20.597	4	1111	84.48

SF: structure factor, F  
 1,111,1111: superlattice reflections  
 9,999,9999: fundamental reflections  
 $m \times 1: F^*F = m \times \{f_{(Ni,Cu)} - f_{Sn}\}^2$   
 $n \times 9: F^*F = n \times \{3f_{(Ni,Cu)} + f_{Sn}\}^2$   
 INTEN: intensity  
 THETA: in degrees  
 L-P: Lorentz-polarization factor  
 MULTI: multi-plicity factor

structure, as described below.

The high temperature phase of the Ni-xCu-25Sn (x=0-30) is reported to have a  $DO_3$  structure [6-9]. To ascertain whether the high temperature phase is indeed the  $DO_3$  structure, the following experiments were performed:

(1) Specimens of the Ni-xCu-25Sn (x: ranging from 10 to 22 at%) alloys were encapsulated in evacuated quartz capsules, kept for 1 hr at  $1000^{\circ}\text{C}$  and then quenched in ice water. The quartz capsules were crushed immediately upon entering the water. Examination of optical micrographs of those quenched specimens did not reveal any evidence of transformation during quenching and the high temperature phase was retained unchanged. It should be mentioned that the  $DO_3$  phase was retained only for  $Ni_3Sn$  alloys containing high amounts of copper. In the case of the Ni-14Cu-25Sn alloy, no  $DO_3$  phase was retained. Instead, a martensite transformation was observed. The details will be described in section 4.4.

(2) A powder specimen of the Ni-17.5Cu-25Sn alloy was made and encapsulated in an evacuated quartz capsule. After annealing at  $1000^{\circ}\text{C}$ , this powder specimen was quenched in ice water without breaking the quartz capsule. The crystal structure of the high temperature phase retained in the quenched, powdered sample was identified by means of X-ray diffractometry, using monochromatic Cu K-alpha radiation. Angles of reflection peaks, measured

and theoretically calculated, are shown in Table 4.2, along with their intensities. As seen in Table 4.2, all the measured reflection angles and their relevant intensities could be consistently explained by assuming a  $DO_3$  structure. Thus, it is certain that the high temperature phase of the Ni-17.5Cu-25Sn alloy has the  $DO_3$  structure. The lattice parameter of the structure was determined to be  $a=5.910\text{\AA}$ . Murakami et al also measured a lattice parameter of the  $DO_3$  phase for  $(Ni,Cu)_3Sn$  as a function of copper composition by X-ray experiments. Their reported data are shown in Figure 4.7. The lattice parameter obtained in the present study is also shown in Figure 4.7 as a large solid circle. As can be seen, the obtained lattice parameter lies on an extrapolated curve of those reported by Murakami et al [7].

Comparing Table 4.2 with Table 4.1, one can index the unidentified reflection peak, 6, Table 4.1 as the  $\{220\}$  reflection of the  $DO_3$  structure. This reflection has the strongest intensity in the  $DO_3$  structure, and therefore, it is possible that a small amount of the high temperature phase might be retained which coexists with the 2H structure in furnace-cooled specimens. However, we still have peak 5, which cannot be identified. Table 4.3 shows reflection angles and intensities calculated by assuming that the  $DO_{19}$  phase is present. As seen from the table, some peaks cannot be indexed by the  $DO_{19}$  structure

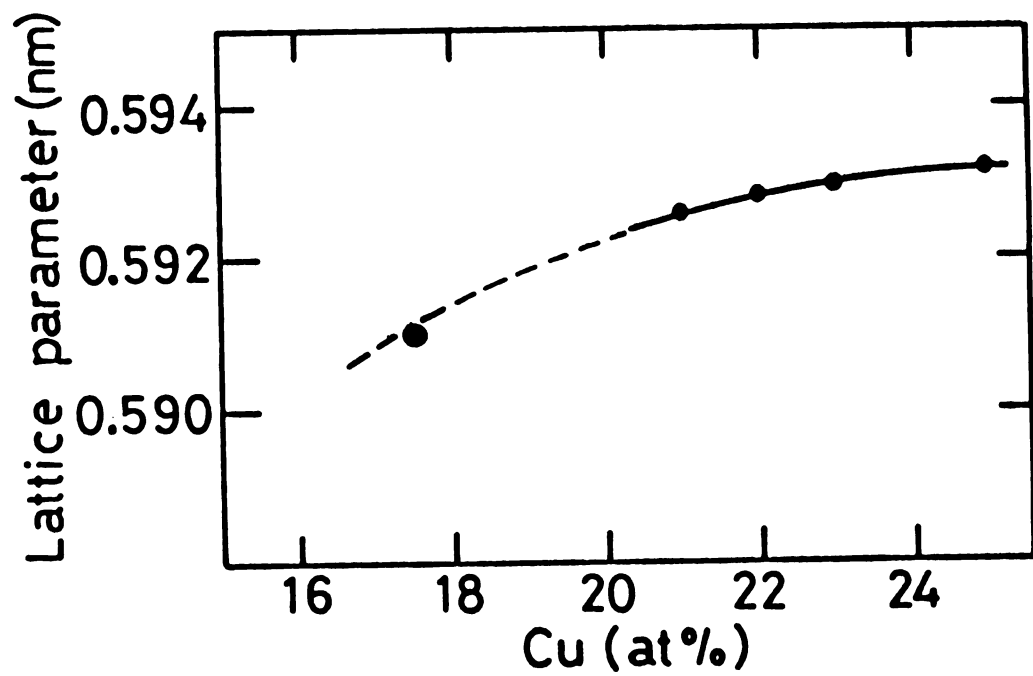


Figure 4.7 Composition dependence of the lattice parameter of  $DO_3$  structure in as-quenched  $Ni-xCu-25Sn$  alloys.

Table 4.2 Angles, d-spacings, and intensities of reflection peaks for a  $DO_3$  structure of a Ni-17.5Cu-25Sn alloy. Lattice parameter used:  $a=5.910\text{\AA}$ ; Cu- $k_{\alpha}$  : 1.54439 $\text{\AA}$ ; Debye-Scherrer method used.

H	K	L	D-SPAC	THETA	INTEN	L-P	MULTI	SF
1	1	1	3.4121	13.08	182.	36.195	8	1111
0	0	2	2.9550	15.15	97.	26.481	6	1111
0	2	2	2.0895	21.69	2123.	12.043	12	9999
1	1	3	1.7819	25.68	90.	8.213	24	1111
2	2	2	1.7061	26.91	26.	7.382	8	1111
0	0	4	1.4775	31.51	325.	5.178	6	9999
1	3	3	1.3558	34.72	70.	4.213	48	1111
0	2	4	1.3215	35.76	32.	3.972	24	1111
2	2	4	1.2064	39.80	647.	3.280	24	9999
1	1	5	1.1374	42.76	21.	2.973	24	1111
3	3	3	1.1374	42.76	7.	2.973	8	1111
0	4	4	1.0448	47.66	229.	2.741	12	9999
1	3	5	0.9990	50.62	34.	2.738	48	1111
2	4	4	0.9850	51.62	34.	2.759	48	1111
0	0	6	0.9850	51.62	4.	2.759	6	1111
0	2	6	0.9345	55.73	429.	2.948	24	9999
3	3	5	0.9013	58.96	18.	3.221	24	1111
2	2	6	0.8910	60.08	19.	3.342	24	1111
4	4	4	0.8530	64.85	173.	4.044	8	9999
1	5	5	0.8276	68.92	51.	4.949	48	1111
1	1	7	0.8276	68.92	25.	4.949	24	1111
0	4	6	0.8196	70.42	27.	5.384	24	1111
2	4	6	0.7898	77.89	2098.	9.137	48	9999

1111: superlattice reflection =  $16(f_A - f_B)^2$   
 9999: fundamental reflection =  $16(3f_A + f_B)^2$

Table 4.3 Angles and intensities of reflection peaks for a  $DO_{10}$  structure of a furnace-cooled Ni-14Cu-25Sn alloy. Lattice parameters used for theoretical calculation:  $a=b=5.306$ ,  $c=4.260\text{\AA}$ ; Cu-k alpha:  $1.544390\text{\AA}$ ; Debye-Scherrer method used.

H	K	L	D-SPAC	INTEN	L-P	MULTI	SF	THETA
1	0	0	4.5951	17.	68.253	6	1	9.65
0	0	1	4.2600	0.	58.263	2	0	10.41
1	0	1	3.1240	42.	30.069	12	111	14.27
1	1	0	2.6530	5.	20.965	6	1	16.87
2	0	0	2.2976	89.	15.118	6	9	19.58
1	1	1	2.2520	17.	14.433	12	111	20.00
0	0	2	2.1300	94.	12.674	2	9999	21.20
2	0	1	2.0222	360.	11.210	12	999	22.39
1	0	2	1.9325	4.	10.057	12	1	23.49
2	1	0	1.7368	10.	7.760	12	1111	26.32
1	1	2	1.6609	2.	6.952	12	1	27.63
2	1	1	1.6083	0.	6.421	24	0	28.61
2	0	2	1.5620	50.	5.974	12	9	29.54
3	0	0	1.5317	3.	5.692	6	1111	30.19
3	0	1	1.4414	0.	4.904	12	0	32.30
0	0	3	1.4200	0.	4.730	2	0	32.85
1	0	3	1.3567	3.	4.244	12	111	34.59
2	1	2	1.3460	9.	4.167	24	1111	34.90
2	2	0	1.3265	14.	4.029	6	9	35.49
3	1	0	1.2745	1.	3.686	12	1	37.18
2	2	1	1.2665	71.	3.636	12	999	37.45
1	1	3	1.2519	3.	3.549	12	111	37.97
3	0	2	1.2436	3.	3.500	12	1111	38.27
3	1	1	1.2210	5.	3.373	24	111	39.11
2	0	3	1.2079	61.	3.304	12	999	39.62
4	0	0	1.1488	9.	3.029	6	9	42.10
2	2	2	1.1260	17.	2.942	12	9	43.16
4	0	1	1.1092	49.	2.885	12	999	43.98
2	1	3	1.0993	0.	2.856	24	0	44.48
3	1	2	1.0936	1.	2.840	24	1	44.77
0	0	4	1.0650	10.	2.774	2	9999	46.32
3	2	0	1.0542	1.	2.756	12	1	46.94
3	0	3	1.0413	0.	2.740	12	0	47.70
1	0	4	1.0375	1.	2.736	12	1	47.94
3	2	1	1.0233	3.	2.728	24	111	48.82
4	0	2	1.0111	14.	2.729	12	9	49.62
4	1	0	1.0027	1.	2.733	12	1	50.19
1	1	4	0.9883	1.	2.749	12	1	51.20
4	1	1	0.9761	3.	2.772	24	111	52.10
2	2	3	0.9693	40.	2.789	12	999	52.62
2	0	4	0.9662	13.	2.798	12	9	52.86
3	1	3	0.9485	3.	2.863	24	111	54.30
3	2	2	0.9448	1.	2.880	24	1	54.61

5 0 0	0.9190	0.	3.038	6	1	56.94
2 1 4	0.9079	4.	3.132	24	1111	58.04
4 1 2	0.9072	1.	3.138	24	1	58.10
5 0 1	0.8984	2.	3.228	12	111	59.02
4 0 3	0.8931	42.	3.288	12	999	59.59
3 3 0	0.8843	1.	3.401	6	1111	60.57
3 0 4	0.8744	2.	3.553	12	1111	61.75
4 2 0	0.8684	60.	3.658	12	9999	62.50
3 3 1	0.8659	0.	3.706	12	0	62.82
0 0 5	0.8520	0.	4.016	2	0	64.70
4 2 1	0.8509	0.	4.045	24	0	64.85
3 2 3	0.8464	4.	4.167	24	111	65.50
5 0 2	0.8438	1.	4.245	12	1	65.90
1 0 5	0.8377	2.	4.445	12	111	66.85
2 2 4	0.8305	18.	4.725	12	9	68.05
5 1 0	0.8253	3.	4.959	12	1111	68.95
4 1 3	0.8191	5.	5.290	24	111	70.11
3 1 4	0.8172	2.	5.403	24	1	70.48
3 3 2	0.8167	3.	5.433	12	1111	70.58
1 1 5	0.8112	3.	5.819	12	111	71.72
5 1 1	0.8102	0.	5.893	24	0	71.93
4 2 2	0.8041	190.	6.443	24	9999	73.31
2 0 5	0.7988	77.	7.057	12	999	74.63
4 0 4	0.7810	41.	11.786	12	9	80.49
5 0 3	0.7715	16.	34.941	12	111	86.72

either. This fact suggests that there is a new phase. As will be shown in the next chapter, the new phase can be identified by precise analysis of electron diffraction patterns. As commonly accepted, electron diffraction is quite powerful in determining complicated crystal structures.

Figures 4.8 and 4.9 show X-ray diffraction patterns obtained from furnace-cooled powder specimens of the Ni-xCu-25Sn (x=14 and 20) alloys. Some of these reflection peaks again could not be indexed by assigning any of the following structures:  $DO_3$ , 2H, or  $DO_{19}$ . Those peaks all correspond to the afore-mentioned unidentified reflection peaks, although they are not consistent regarding reflection intensity.

Figures 4.6, 4.8, and 4.9 suggest a possibility of the existence of a new phase. These three figures all seem to contain the  $(220)_{DO_3}$  reflection peak, although the reflection angle of the peak is slightly different. Intensities for the peak, however, appear to increase with increasing Cu content, suggesting that the volume fraction of the retained  $DO_3$  structure increases with increasing copper content. (Intensity calculations for reflection lines of the 2H,  $DO_3$  and  $DO_{19}$  structures shown in Tables 4.1-4.3 were carried out by using a Dec 20 computer.)

Table 4.4 shows the results obtained by Debye-Scherrer method for the furnace cooled Ni-xCu-25Sn(x=14 and

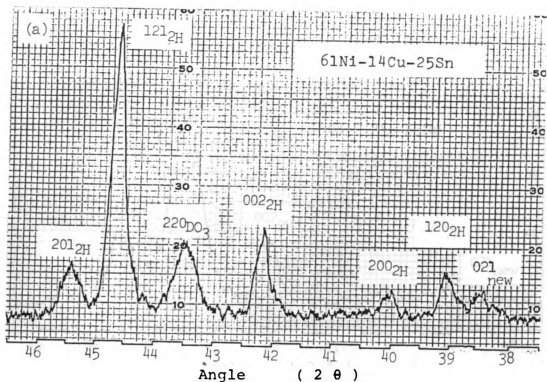


Figure 4.8 Partial diffractometer pattern of a furnace-cooled Ni-14Cu-25Sn alloy.

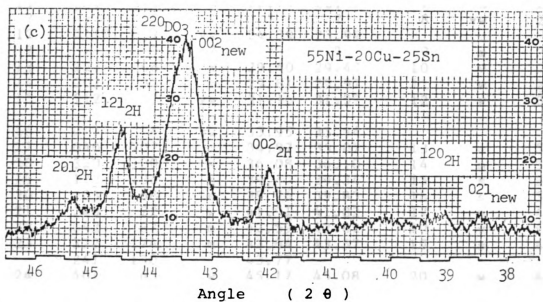


Figure 4.9 Partial diffractometer pattern of a furnace-cooled Ni-20Cu-25Sn alloy.

Table 4.4 Debye-Scherrer data obtained from the alloys, furnace-cooled from 1000°C. Cu-k alpha used.

peaks	hkl	Ni-14Cu-25Sn				Ni-17.5Cu-25Sn		
		intensity (cal)	intensity (meas)	theta(degree) (cal)	theta(degree) (meas)	peaks	intensity (meas)	theta (meas)
1	110	8	w	12.91	13.07	1	vw	13.10
2	011	11	w	13.30	13.45			
3	101	7	vw	14.39	14.75			
4	020	18	w	16.65	16.95			
	111	5		16.67				
5	x	?	w	?	19.00			
6	120	56	m	19.51	19.55	2	m	19.50
7	200	27	m	20.06	20.15	3	m	20.13
8	002	103	s	21.09	21.14	4	s	21.15
9	x	?	s	?	21.86	5	vs	21.77
10	121	289	vs	22.29	22.42	6	vs	22.40
11	201	141	s	22.79	22.87	7	m	22.90
?	x	?	?	?	?	8	vw	23.07
12	211?	7	vw	24.39	23.99			
?	x	?	?	?	?	9	m	25.70
13	122	66	m	29.40	29.47	10	w	29.28
14	202	32	m	29.81	29.97	11	w	29.85
15	212	7	vw	31.16	31.37	12	w	31.45
16	013	4	vw	33.95	33.94			
17	040	207	m	34.97	35.07	13	m	34.92
18	320	100	s	36.08	36.10	14	m	36.04
19	123	136	s	39.40	39.34	15	s	39.24
20	203	68	s	39.76	39.83	16	s	39.88
21	240	22	w	41.91	41.82	17	w	41.77
22	042	87	m	42.59	42.62	10	w	42.39
23	322	174	m	43.64	43.57	19	s	43.55
	241	130		43.77				
24	401	65	w	45.17	45.08	20	w	45.20
25	004	43	w	46.03	46.16	21	w	46.00
26	242	45	m	49.35	49.34	22	m	49.16
27	402	23	w	50.77	50.95			
28	124	48	w	52.50	52.64			
	204	24		52.86				
29	x	?	vw	?	55.98	23	w	55.77
30	243	183	m	59.10	58.99	24	m	58.86
?	x	?	?	?	?	25	m	59.86
31	403	99	w	60.71	60.48	26	m	60.31
?	160	34	?	61.16	?			

peaks	hkl	Ni-14Cu-25Sn				Ni-17.5Cu-25Sn		
		intensity (cal)	intensity (meas)	theta(degree) (cal)	theta(degree) (meas)	peaks	inten (meas)	theta (meas)
32	413	3	w	62.11	62.31			
	304	6		62.12				
	432	9		62.28				
33	440	38	w	63.28	63.44	27	m	63.17
	161	227		63.41		28	m	63.51
?	351	13	?	64.09	?			
?	520	41	?	64.61	?	29	w	64.59
34	015	7	m	65.53	65.27			
35	441	257	w	65.66	65.51	30	s	65.33
36	105	6	w	66.21	66.51	31	w	66.68
	423	11		66.63				
37	044	183	w	66.82	66.83	32	m	66.80
38	521	279	m	67.09	67.79	33	m	67.81
39	324	400	w	68.30	68.26	34	m	68.10
?	162	121	?	71.24	?	35	s	72.94
40	125	429	m	73.49	73.00			
41	205	226	m	74.14	73.65	36	s	73.54
	442	153	m	74.33				
42	x	?	w	?	75.73	37	m	75.74
43	522	183	w	76.49	76.33	38	m	76.63
44	x	?	w	?	78.17	39	w	77.98
45	244	229	vw	78.83	78.81	40	w	78.41

17.5at%) alloys. Measured intensities are denoted by the following indications: vw(very weak), w(weak), m(medium), s(strong) and vs(very strong). From these data, a new phase is known to coexist with the 2H and  $DO_3$  phases in  $(Ni,Cu)_3Sn$  alloys when they are furnace-cooled. Most of the observed reflection lines can be indexed by assigning the 2H structure, while some of them cannot be indexed even by assigning the  $DO_3$ , 2H, and  $DO_{19}$  structures.

The X-ray diffraction data obtained by both the Debye-Scherrer method and the diffractometer method were in very good agreement each other. However, the results obtained in the present study are inconsistent with the reports by Murakami et al [7-9], which clearly stated that, in the range of copper contents between 8 and about 18 at%, the 2H phase is the only one present at temperatures below  $700^{\circ}C$ .

### 4.3 Microstructures in Furnace-cooled Specimens

As shown in previous sections, X-ray diffraction data and optical micrographs clearly indicate that there is another phase in addition to the 2H phase in furnace-cooled specimens of the three Ni-xCu-25Sn alloys (x=14, 17.5, and 20). In this section the crystal structure of this proposed, new phase will be identified by means of electron diffraction. Also, results of detailed examinations of microstructures for furnace-cooled specimens will be shown.

Disks of the Ni-xCu-25Sn alloys (x=14 and 20) were encapsulated in evacuated quartz capsules and annealed at 1000°C, where the high-temperature DO<sub>3</sub> phase is known to be stable. The disks were kept at this temperature for about 1 hr, then furnace-cooled.

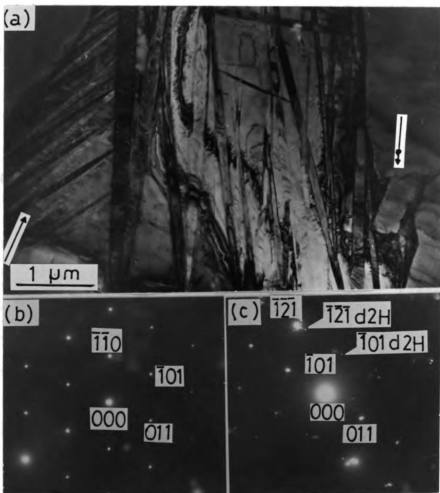
The transmission electron microscopes primarily used in this study were Hitachi HU-200F and H800 microscopes, which were operated at 200 keV. A Kratos EM 1500 microscope located at National Center for Electron Microscopy, Berkeley, CA was also used for some work. This microscope was operated at 1500 keV.

#### 4.3.1 Microstructures of a Furnace-cooled Ni-14Cu-25Sn Alloy

Figure 4.10(a) is an electron micrograph, showing a typical microstructure of the furnace-cooled alloy. In the figure, two distinct regions are seen. One is a region composed of bands. This region is surrounded by an irregularly curved boundary. These bands are seen to contain densely-packed internal structures, whose contrasts resemble ones for either thin twins or stacking faults. The bands are bounded by slightly dislocated areas, which have the same crystal orientation. This can be known from the continuation of bend contours. Because bands vary in size and orientation, regions containing bands are very complicated. To clarify relations further between the bands and the associated areas of dislocations, a part of Figure 4.10 was enlarged.

The enlarged micrograph is shown by the single-headed arrow in Figure 4.10(a). A brief survey of this area leads one to the incorrect idea that three bands form one spear, as often reported for Cu-Al-Ni alloys [32]. In the case of the Cu-Al-Ni alloy, the spear consists of two 2H martensite variants. The side bands have twin-like internal structures, while the center one has no such internal structure, but contains a dislocated structure. It is clear then that this spear-like structure is

Figure 4.10 Microstructure of a Ni-14Cu-25Sn specimen, furnace-cooled from 1000°C. (a) bright field image of 2H and d2H phases. (b) diffraction pattern, taken from the top left-hand side of a 2H region:  $[1\bar{1}1]$  zone axis. (c) diffraction patterns, taken from the central region of the micrograph:  $[1\bar{1}1]$  zone axis for 2H and d2H. (d) angles between two reflection spots.



(d)

$g_i \cdot g_j$	angle(degrees)		
	2H	d2H	obs.
$011 \cdot 110$	66.5	72.3	72
$011 \cdot 101$	55.5	52.0	54
$110 \cdot 101$	58.0	55.8	54

different from those observed in the Cu-Ni-Al alloy. It can be seen in Figure 4.11 that the bands with twin-like internal structures and areas with dislocations are alternatively formed.

The other region shows a slightly different microstructure that contains a low density of dislocations. The morphology of this region is essentially the same as that of dislocated areas shown above. Figure 4.12 is an enlarged micrograph of an area pointed by the double-headed arrow in Figure 4.10(a). It can be seen in Figure 4.14 that a sub-boundary was constructed by dislocation networks. In the area enclosed by the networks, one can see typical fringe contrasts of stacking faults. These stacking faults are considered to have been formed by dissociation of boundary dislocations.

Figure 4.13 is a high magnification electron micrograph of another furnace-cooled Ni-14Cu-25Sn specimen. Diffraction patterns were taken from a large, bright area in the upper right-hand side of the micrograph. It was found that the crystal structure of the area is a 2H structure. There is a low-angle boundary, consisting of at least two sets of dislocation arrays which run from the top left-hand side to the bottom right-hand side of the micrograph. In bright areas of the 2H phase, dislocation loops and vacancy loops are seen.

Figure 4.11 Enlarged micrograph of an area indicated  
by the single-headed arrow in Figure 4.10.

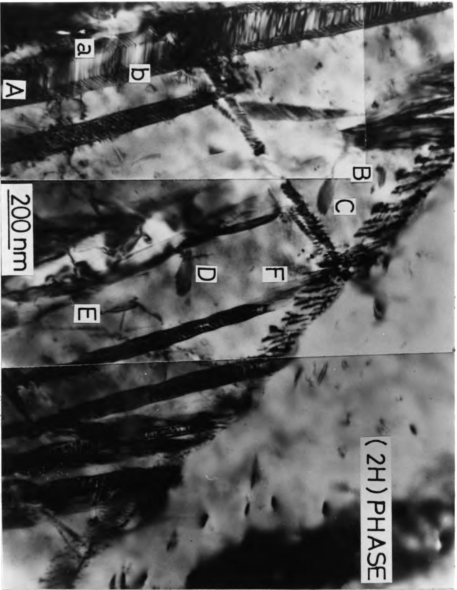


0.5 μm

**Figure 4.12** Enlarged micrograph of an area indicated by the double-headed arrow in Figure 4.10. Note fringes of stacking faults and dislocation networks in a 2H region.



Figure 4.13 High magnification micrograph of a furnace-cooled Ni-14Cu-25Sn specimen, showing many microstructural features.



These loops are thought to be associated with the formation of the fine bands seen in Figure 4.13. These fine bands were found to be a new phase having a distorted 2H structure, which is slightly different from that of the normal 2H phase. Identification of this new phase will be described in section 4.3.3. It should be noted that the distorted 2H phase has not been observed to cut across low-angle boundaries.

Two noticeable microstructural features are seen in Figure 4.13. One is the band denoted by A; the other is in the areas denoted by B, C, D, and E. The former microstructure clearly reveals characteristics similar to those of the bands formed in furnace-cooled specimens. Close inspection of band A discloses that the band is thick and contains many planar faults. These planar faults were probably formed when bands nucleated in regions of the  $DO_3$  phase. From the appearance of the bands seen in Figure 4.13, it is obvious that the bands of distorted 2H phase grew to hold orientation relationships with its  $DO_3$  parent phase. From band A, one knows that the other bands seen in Figure 4.13 are similar but their width is not so large as those for marked regions 'a' and 'b' in band A. Therefore, the contrast of those bands appears complicated.

The other microstructural feature in Figure 4.13 is one that demonstrates the nucleation process of bands.

Close observation of areas C and D in particular shows that each area contains striations oriented in two directions. Either of the directions is parallel to each other in the two areas. Microstructures in areas C, D, and E are otherwise very similar to those observed in nuclei of a martensite in a AuCd alloy studied by Mukherjee et al [16]. It should be noted that these striations are not parallel to the stacking faults observed in bands A.

In Figure 4.13, it can be seen that the upper right-hand side of the figure does not contain any band structures, while the lower part contains many bands of varying size that exhibit stacking faults. These two areas are divided by dislocation networks that create a low-angle boundary. Because the areas have the same 2H structure, and their crystal orientation is almost the same, it is necessary to explain their microstructural differences. The explanation can be made by considering the following phase decomposition that may occur during furnace-cooling of  $(\text{Ni,Cu})_3\text{Sn}$  alloys:

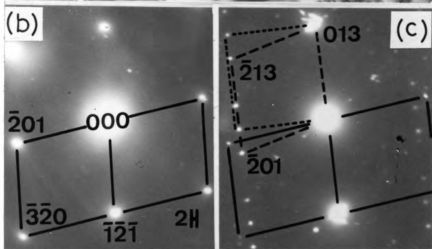
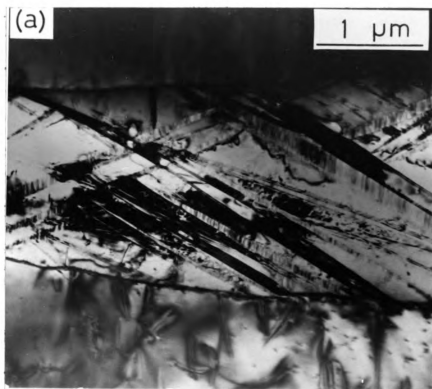


where d2H is the distorted 2H phase. Areas of the 2H structure transformed at high temperatures from the  $\text{DO}_3$  phase are denoted as 2H(1), and areas later transformed to

the 2H structure at lower temperatures is denoted as 2H(2). Their lattice parameters differ slightly from each other, both because of diffusion processes and because the phase boundary involved is probably parallel to the composition axis of the composition-temperature phase diagram. The dislocation networks seen in Figure 4.13 are, therefore, thought to have been formed to accommodate lattice misfit between those two 2H regions. In other words, low angle boundaries are probably original phase boundaries between 2H(1) and  $DO_3$  regions.

Figure 4.14 (a) is an electron micrograph of a furnace-cooled Ni-14Cu-25Sn specimen. Because this figure is a low magnification photograph, macrostructural differences are clearly seen between a two-phase region with many bands and regions with dislocations. Diffraction patterns taken from a lower region with dislocations and a central region with bands corresponding to Figure 4.14(b) and (c), demonstrate that the latter banded region is composed of two phases, the 2H phase and the new distorted 2H phase. More importantly, the 2H phase in the central two-phase region has nearly the same crystal orientation as that of the lower region with dislocations; the foil normals of those regions are analysed to be the  $[2\bar{3}4]$  zone axis. This result is consistent with the observations of dislocation networks seen in Figure 4.13.

Figure 4.14 Microstructure of a Ni-14Cu-25Sn specimen, furnace-cooled from 1000°C. (a) bright field image of 2H and d2H phases. (b) diffraction pattern of  $[2\bar{3}4]$  zone axis taken from a 2H region. (c) diffraction patterns taken from a two-phase region.



It should be noted that the diffraction patterns taken from the central region contain two other zone axes, marked as dotted lines in Figure 4.14(c). Inspection of the diffraction patterns for these zone axes demonstrate that they are for two variants that appear as bands in the central region. The crystal structure of the variants will be identified in section 4.3.3.2.

Figure 4.15(a) is another micrograph taken from the same specimen as that used for Figure 4.14. A two-phase area with variants is seen to be enclosed by dislocation networks in which surface etching is evident. 2H regions are also seen within the enclosed area. Figure 4.15(b) is a diffraction pattern, taken from a region within the enclosed area having bands. It was found that streaks in Figure 4.15(b) are all perpendicular to fine microstructures in bands.

Figures 4.16(a),(b), and (c) are high magnification micrographs, taken from the framed areas, A, B, and C, in Figure 4.15(a), which show detailed microstructures of the low-angle boundaries. These boundaries are zigzag and, as was seen in Figures 4.10 and 4.14, no bands cross these zigzag low-angle boundaries. Striations clearly seen in Figures 4.16(a), (b), and (c) are parallel to each other, and are perpendicular to streaks in the diffraction pattern in Figure 4.15(b). These striations are stacking faults that were formed as lattice invariant strain. This

Figure 4.15 Microstructure of a Ni-14Cu-25Sn specimen, furnace-cooled from 1000°C. (a) bright field image of 2H and d2H phases. (b) diffraction pattern taken from an area containing bands.

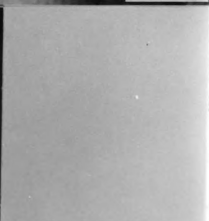
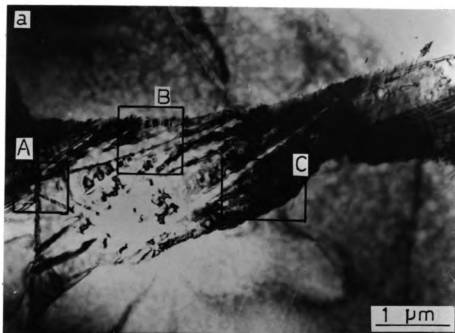
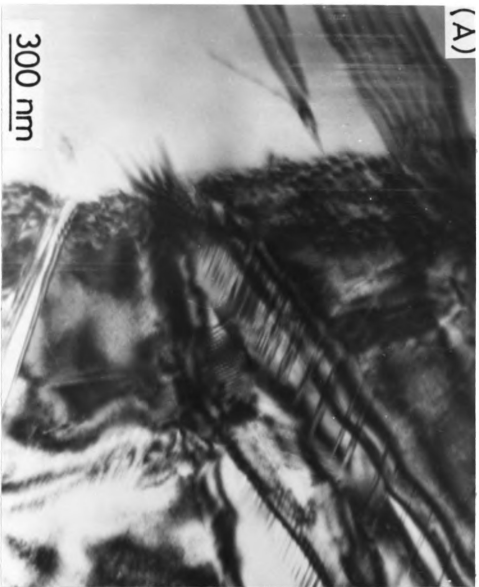


Figure 4.16 High magnification micrographs taken,  
(a) from area A; (b) from area B; and  
(c) from area C in Figure 4.15.

(A)



300 nm

Figure 4.16 High magnification micrographs taken,  
(b) from area B in Figure 4.15.

(B)



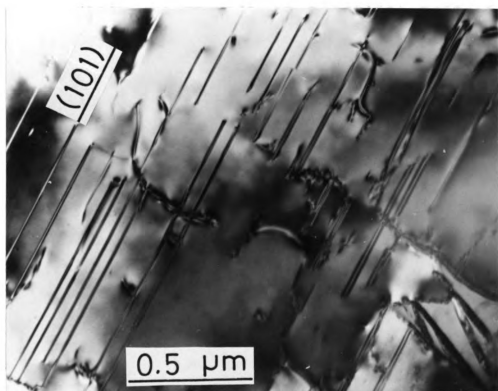
Figure 4.16 High magnification micrographs taken,  
(c) from area C in Figure 4.15.



invariant strain is necessary for the new phase to nucleate and grow in the  $DO_3$  matrix. Figure 4.16(a) shows a moire fringe pattern, indicating complication of this microstructure; the nature of the moire fringe pattern is not clarified.

In Figures 4.10 to 4.16, focus was placed on microstructural features of the new phase, formed as bands in the furnace-cooled Ni-14Cu-25Sn. Note, however, that dislocated areas of 2H-phase are predominant. A typical example of a 2H-phase area which demonstrates dislocations and thin planar faults is shown in Figure 4.17. Trace analysis revealed that the thin planar faults were on (101) planes, one of the two twin planes that were reported for 2H martensite by Pak[6] and Ostuka[32].

Figure 4.17 Electron micrograph of a 2H region taken from a Ni-14Cu-25Sn specimen, furnace-cooled from 1000°C. Note (101) planar faults.



#### 4.3.2 Microstructural Morphology of a Furnace-cooled Ni-20Cu-25Sn Alloy

Specimens of this alloy were annealed at 1000°C and furnace-cooled. Figure 4.18 is a typical example of microstructures obtained in the specimens. It can be seen from this figure that bands contain internal faults and occur in a zigzag form. Areas bounded by these bands are heavily bent by buckling in thin areas possibly caused by the elastic strain field between a band and the neighbor area.

Figure 4.18 also shows many dislocations at or near low-angle boundaries, in which the new phase nucleated or by which the new phase was blocked to grow; these dislocations are considered to be transformation dislocations generated to accommodate transformation strain. A narrow band was probably formed after wide bands were formed at higher temperatures.

The micrograph shown in Figure 4.19 demonstrates that the microstructural morphology in the right-hand side of this figure is similar to that observed in Figure 4.18. Bands in Figure 4.19 also exhibit a zigzag form. Bands are known to have a certain width from the number of boundary fringes. It is interesting that both dislocation lines and loops are seen, marked by the single-headed arrows. More important is the microstructure seen in the

Figure 4.18 Bright field image of a Ni-20Cu-25Sn specimen, furnace-cooled from 1000°C to room temperature. Note dislocations and planar faults in 2H regions and planar faults in d2H regions.



Figure 4.19 Bright field image of a Ni-20Cu-25Sn specimen, furnace-cooled from 1000°C, showing zigzag bands.



left hand-side of the figure. Here, wide bands coexist with uniformly distributed internal faults. These wide bands formed alternately with dislocated areas. In the dislocated areas, there are small-sized 2H bands showing no internal faults. Some dislocations are also found in internally faulted bands, marked by the double-headed arrow.

A relation between wide bands with fine internal faults and narrow, zigzag bands within dislocated areas is shown in Figure 4.20. From this figure and optical micrographs taken from furnace-cooled specimens, one can see that the wide bands correspond to the rod-shaped structure containing fine twins, while the zigzag bands within dislocated areas correspond to areas surrounded by the rod-shaped structures.

Differences in microstructural features between the two Ni-xCu-25Sn ( $x = 14$  and  $20$ ) alloys are summarized as follows: (1) the volume fraction of the 2H phase to the new phase is lower in the Ni-20Cu-25Sn alloy than in the Ni-14Cu-25Sn alloy, suggesting the location of phase boundaries for these two phases, and (2) the 2H phase has a larger number of (101) planar faults in the Ni-20Cu-25Sn alloy, while the 2H phase has a fewer faults in the Ni-14Cu-25Sn alloy, suggesting a relative change in lattice parameters of the 2H and the new phase as a function of copper content. No detailed observations of the lattice

Figure 4.20 Bright field image of a Ni-20Cu-25Sn specimen, furnace-cooled from 1000°C to room temperature. Note many dislocation loops and dislocation lines in 2H regions.



parameter changes were made.

#### 4.3.3 Identification of Phases by Electron Diffraction

Electron diffraction was used to investigate the crystal structures of both the banded and the slightly dislocated regions which were formed in the Ni-14Cu-25Sn alloy that was furnace-cooled from 1000°C.

##### 4.3.3.1 Crystal Structure of Slightly Dislocated Regions

Figure 4.21 shows four zone axes of selected-area diffraction patterns taken from slightly dislocated regions. It is seen that all the diffraction patterns can be indexed by assigning the 2H structure ( $\gamma$ -Cu<sub>3</sub>Ti-type) which has lattice parameters of  $a=4.495\text{\AA}$ ,  $b=5.380\text{\AA}$ , and  $c=4.285\text{\AA}$ , as measured in X-ray experiments. The four zone axes in Figure 4.21 are known to be  $[100]$ ,  $[2\bar{1}0]$ ,  $[0\bar{1}1]$ , and  $[0\bar{1}2]$ . The slightly dislocated regions are found to be the 2H phase.

##### 4.3.3.2 Crystal Structure of Banded Regions

The crystal structure of the banded regions (a new phase) was also identified. Figure 4.22 shows three selected-area diffraction patterns taken from banded

Figure 4.21 Electron diffraction patterns taken from 2H areas of Ni-14Cu-25Sn specimens furnace-cooled from 1000°C. Zone axes: (a) [100]; (b) [2 $\bar{1}$ 0]; (c) [0 $\bar{1}$ 1]; and (d) [0 $\bar{1}$ 2].

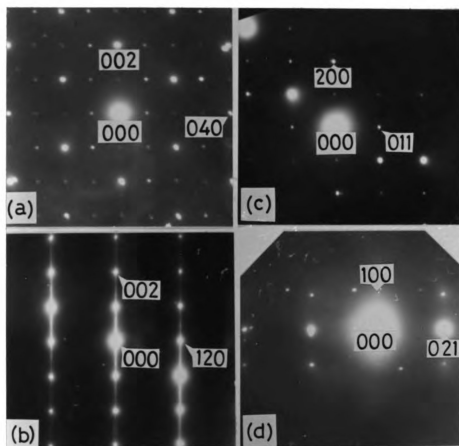
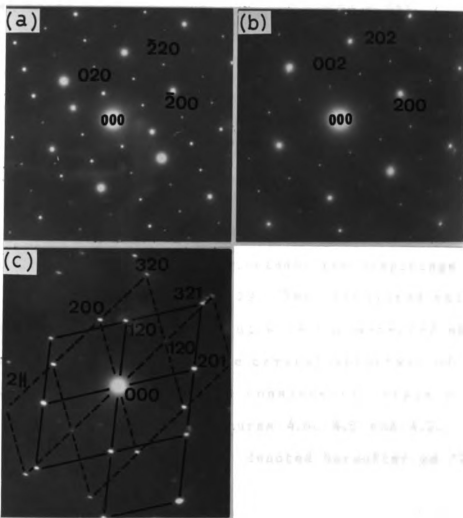


Figure 4.22 Electron diffraction patterns taken from d2H areas of Ni-14Cu-25Sn specimens furnace-cooled from 1000°C. Zone axes: (a) [001]; (b) [010]; and (c) [001] and  $[2\bar{1}4]$ .



regions. These three diffraction patterns contain a-, b-, and c-axes; these three axes are not perpendicular to each other. From the three diffraction patterns, the three angular lattice parameters can be measured and are as follows:  $\alpha = 85^\circ$ ,  $\beta = 86^\circ$ , and  $\gamma = 84^\circ$ .

By adopting these angular lattice parameters and the unit cell lengths estimated as  $a=4.53\text{\AA}$ ,  $b=5.31\text{\AA}$ , and  $c=4.34\text{\AA}$ , one can index all the diffraction patterns shown in Figures 4.22(a,b,c) under the assumption that the atomic arrangement of the new phase is the same as that of the 2H phase. Tables 4.5 and 4.6 show the calculated d-spacings and angles used for indexing diffraction patterns in Figure 4.22. The table also includes the d-spacings and angles measured from Figure 4.22. The calculated values are seen to be in good agreement with the measured ones. It should be mentioned that the crystal structure of the new phase identified here can consistently explain the unidentified X-ray peaks in Figures 4.6, 4.8 and 4.9. The crystal structure identified is denoted hereafter as d2H.

Table 4.5 D-spacings of the d2H phase

hkl	d-spacing
010	5.25
100	4.46
001	4.27
110	3.62
011	3.45
101	3.18
020	2.62
111	2.92
120	2.39
021	2.32
200	2.23
121	2.19
210	2.15
002	2.14
012	2.04
201	2.03
211	1.99
102	1.97
112	1.93
203	1.22

Table 4.6 Angles between two planes for d2H and 2H structures

	$(h_1k_1l_1) \cdot (h_2k_2l_2)$	observed angles	d2H	2H
Figure 4.22(a)	$010 \cdot \bar{1}00$	84	84	90
[001] zone	$010 \cdot \bar{1}10$	46.5	45.6	50
	$100 \cdot \bar{1}20$	55	54.4	59.1
Figure 4.22(b)	$001 \cdot 100$	85	86	90
[010] zone	$201 \cdot 100$	26	26.8	27.7
	$001 \cdot 101$	42	42.1	43.6
Figure 4.22(c)	$120 \cdot 201$	70	70.4	63
$[\bar{2}\bar{1}\bar{4}]$ zone	$201 \cdot 321$	32	31.8	28.9

#### 4.4 Microstructure and the Crystal Structure of As-Quenched (Ni,Cu)<sub>3</sub>Sn Alloys

Several (Ni,Cu)<sub>3</sub>Sn alloys were quenched from 1000°C to ice water in an attempt to retain the high-temperature DO<sub>3</sub> phase and its product phase. However, even with a very rapid quenching by crushing the encapsulated quartz tubes in ice water, no dual phases could be retained. For alloys containing Cu ranging from 16 to 22 at%, the high-temperature DO<sub>3</sub> phase was retained, whereas for an alloy with a copper content of 14 at% Cu, a martensite was formed as a product phase of the DO<sub>3</sub> phase. These observations disagree with data reported by Murakami et al [7-9].

Figure 4.23 is an optical micrograph of the quenched Ni-14Cu-25Sn alloy, showing a plate-like martensite. This martensite reveals fine striations, indicating fine planar structures. Bright and dark bands are martensite variants, and no parent DO<sub>3</sub> phase is seen. The microstructure of the martensite bears resemblance to that of the thermoelastic martensite in a Cu-Ni-Al alloy[32]. However, the martensite formed in the Ni-14Cu-25Sn alloy did not show any thermoelastic characteristics. Detailed microstructures of the martensite are seen in transmission electron micrographs.

Figure 4.24 is an electron micrograph of a martensite

Figure 4.23 Optical micrograph of a Ni-14Cu-25Sn specimen, quenched from 1000°C to ice water, showing a plate-like martensite formed from a DO<sub>3</sub> phase.

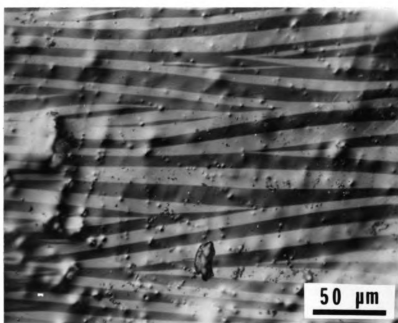
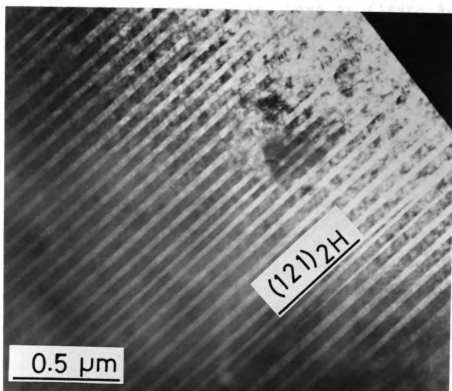


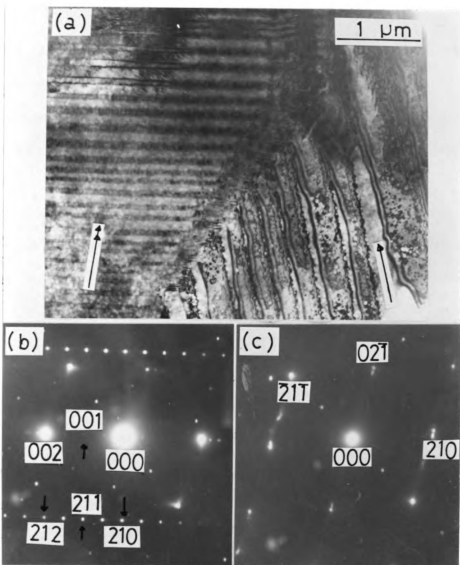
Figure 4.24 Electron micrograph of a 2H martensite (denoted as 2H') formed in a Ni-14Cu-25Sn specimen, quenched from 1000°C to ice water. Note a high density of (121) twins.



with a high density of microtwins. Trace analysis of the micrograph showed that the twinning plane was the (121) plane of the 2H structure. As will be shown below, the crystal structure of the martensite was identified to be the 2H structure.

A similar microstructure is shown in Figure 4.25(a), where two martensite variants are present. The diffraction pattern taken from the area indicated by the single-headed arrow in the figure is shown in Figure 4.25(b). Figure 4.25 (c) is taken from the area by the double-headed arrow. Both can be indexed as  $[\bar{1}20]$  and  $[\bar{1}24]$  by assigning them the 2H structure. Several other diffraction patterns were also obtained from the martensites and all could be indexed by the 2H structure. To obtain further details of the martensite microstructure, diffraction patterns were taken from a martensite variant located in the upper portion of the micrograph. Figure 4.25(c) represents the diffraction patterns thus obtained, which clearly exhibit a twinning relationship. Twin planes in Figure 4.25(a) were found to be the  $(121)_{2H}$  twins, as observed in Figure 4.24. Some (121) twins in the present alloy contain fine striations, which are stacking faults.

Figure 4.25 Microstructure of an as-quenched Ni-14Cu-25Sn specimen, showing two martensite variants containing twins. (a) bright field. (b) diffraction pattern of  $[\bar{1}20]$  zone of 2H, taken from an area indicated by the single-headed arrow. (c) diffraction pattern of  $[\bar{1}24]$  zone, taken from an area indicated by the double-headed arrow.



## 4.5 Aging Effects of the Ni-20Cu-25Sn Alloy

### 4.5.1 Results

The X-ray and electron diffraction analyses have revealed that either the two phases, 2H and d2H, or the three phases, 2H, d2H, and  $DO_3$ , are formed in Ni-xCu-25Sn alloys (x ranging between 14 and 20 at%) when they are furnace-cooled from  $1000^\circ\text{C}$ . Because of this heat treatment, however, no transformation temperatures from the  $DO_3$  phase to the 2H and d2H phases are known. To obtain information about transformation temperatures, aging studies were carried out. The alloy had a Cu content of 20 at%, and it was quenched from  $1000^\circ\text{C}$  to retain the high temperature  $DO_3$  phase. Samples were then aged for 24 hr at  $650^\circ$ ,  $600^\circ$ ,  $500^\circ$ , and  $350^\circ\text{C}$ . After these aging treatments, the specimens were again quenched in ice water and investigated by X-ray diffractometer.

In the case of the  $650^\circ\text{C}$  aging, no phase transformation of the retained  $DO_3$  phase was found to have taken place. In the range of angles (theta in degree) between 18 and 60, only three sharp reflection peaks were observed at angles of  $21.69^\circ$ ,  $25.57^\circ$ , and  $47.37^\circ$ . By comparing with Table 4.2, these angles were indexed as the fundamental reflections of the  $DO_3$  structure, 022, 113, and 044. Figure 4.26 shows the portion of X-ray

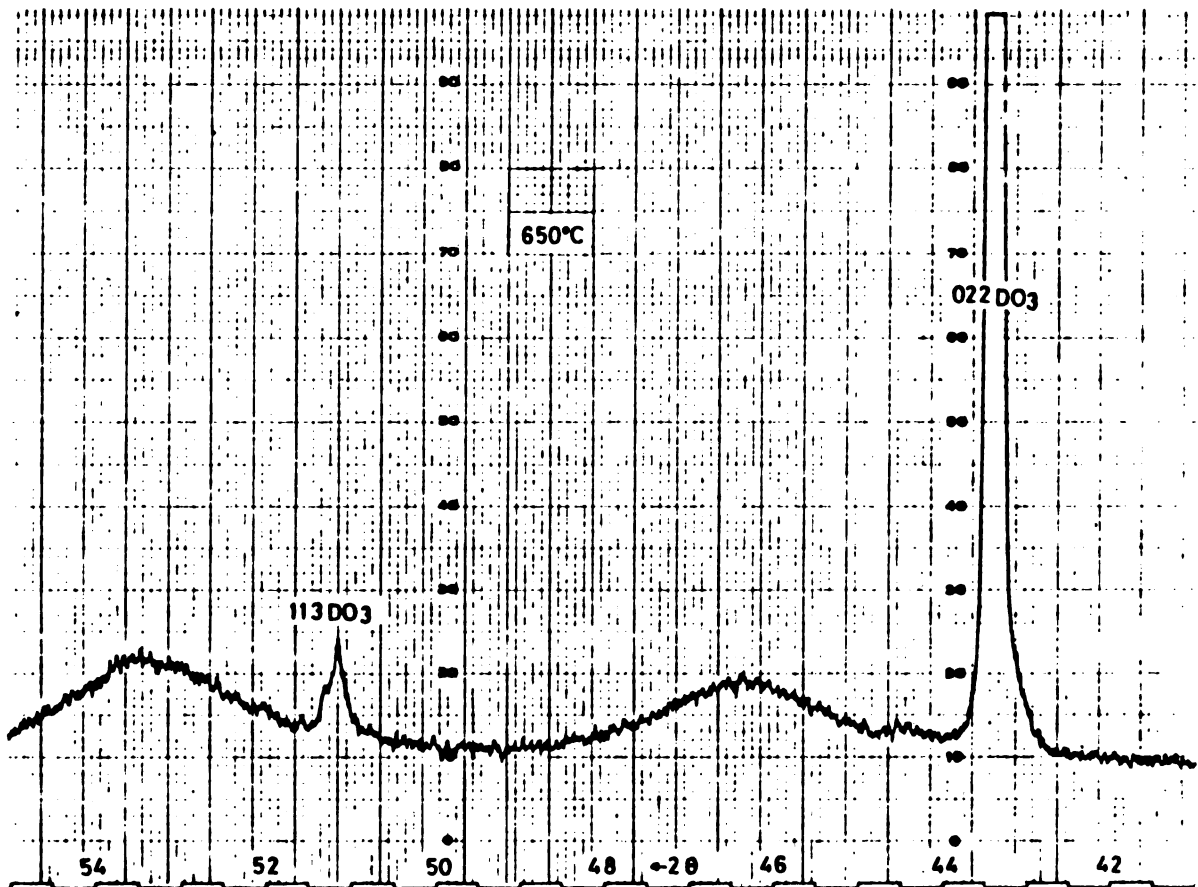


Figure 4.26 Partial diffractometer pattern of a Ni-20Cu-25Sn alloy, quenched in ice water from 1000°C aged 24 hr at 650°C, and quenched in ice water.

diffraction pattern obtained from a specimen aged at 650°C, which presents the strongest 002 peak of the DO<sub>3</sub> structure. As seen in this figure, two broad peaks were also observed, which appeared at angles of approximately 23.2 and 26.7°. These peaks were found not to be indexed by assigning them to any of the crystal structures already known in this present study.

On the other hand, in the case of the 500°C aging, the phase transformation of the DO<sub>3</sub> into the 2H phase is evident. The reflection peaks observed from an aged specimen are listed in Table 4.7, which can all be indexed by both the DO<sub>3</sub> and the 2H structures. In Figure 4.27, a portion of X-ray data is shown, whose angle range is corresponding to that for Figure 4.26. As seen in these figures, their aging behavior is evidently different.

For a specimen aged at 600°C, essentially the same transformation was observed as that obtained from the specimen aged at 500°C; both the 2H and the DO<sub>3</sub> phases are seen to coexist at 600°C (Table 4.8). Note that all reflection peaks in the table can be indexed by assigning them to the DO<sub>3</sub> and the 2H structures, although some discrepancies are seen in the intensities of the peaks. Comparing angles shown in Tables 4.7 and 4.8 with angles listed in Table 4.1, it is also seen that the lattice parameters of the 2H phase formed in the alloy with a Cu content of 20at% are the same as for the alloy with a Cu

Table 4.7 X-ray reflection peaks observed  
in a specimen aged 24hr at 500°C.

Number of peaks	Angle( $\theta^\circ$ ) measured	Intensity measured	Index
1	15.12	vw	200(DO <sub>3</sub> )
2	19.50	vw	120(2H)
3	19.93	w	200(2H)
4	21.16	s	002(2H)
5	21.63	vvs	022(DO <sub>3</sub> )
6	22.29	m	121(2H)
7	22.88	m	201(2H)
8	26.80	vs(?)	222(DO <sub>3</sub> )
9	31.38	vvs	004(DO <sub>3</sub> )
10	34.92	w	133(DO <sub>3</sub> )
11	39.56	s	224(DO <sub>3</sub> )
12	42.45	m	115,333(DO <sub>3</sub> )

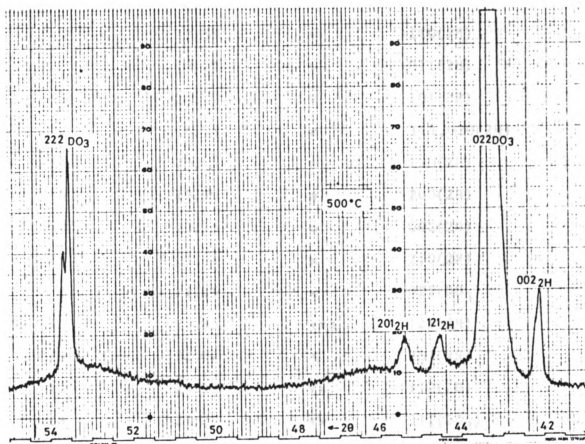


Figure 4.27 Partial diffractometer pattern of a Ni-20Cu-25Sn alloy, quenched in ice water from  $1000^\circ\text{C}$  aged 24 hr at  $500^\circ\text{C}$ , and quenched in ice water.

Table 4.8 X-ray reflection peaks observed  
in a specimen aged 24hr at 600°C.

Number of peaks	Angle( $\theta^\circ$ ) measured	Intensity measured	Index
1	12.83	w	110(2H)
2	13.22	w	011(2H)
3	14.27	w	101(2H)
4	16.58	m	111,020(2H)
5	19.40	m	120(2H)
6	19.90	m	200(2H)
7	20.95	m	002(2H)
8	21.54	m	210(2H)
9	21.65	w	022(DO <sub>3</sub> )
10	22.35	vvs	121(2H)
11	22.62	m	201(2H)
12	24.92	vw	112(2H)
13	25.25	vw	311(DO <sub>3</sub> )
14	29.20	w	122(2H)
15	29.60	w	202(2H)
16	34.80	w	040(2H)
17	34.91	vw	133(DO <sub>3</sub> )
18	35.80	w	320(2H)
19	39.14	w	123(2H)
20	39.47	w	203(2H),224(DO <sub>3</sub> )

content of 14at%.

Another aging experiment was also made at 350°C in an attempt to observe the d2H phase. The X-ray data obtained from this sample show the presence of the d2H phase, as shown in Figure 4.28. All reflection peaks were very broad, and the intensities are not strong. Only  $(121)_{d2H}$  and  $(022)_{D03}$  peaks are clearly identified. Also, electron diffraction analysis of specimens aged at 350°C was carried out, and the presence of the d2H phase was revealed. An example of the diffraction patterns is shown in Figure 4.29.

#### 4.5.2 Discussion of Aging Results

With the 650°C aging, only a few sharp reflection peaks were observed, in addition to two broad lines. Because coarse-grained specimens were used for the X-ray diffractometer experiment, the appearance of fewer peaks may have been caused by preferential orientation of grains that grew during the aging. The line broadening phenomena are more interesting; the presence of the broad lines indicates that some phase decomposition or some pre-transformation might occur at 650°C prior to the phase transformation from the  $D0_3$  to the 2H phase. Transmission electron microscopy and diffraction analysis of specimens aged at 650°C for 20 hr support the idea that a spinodal

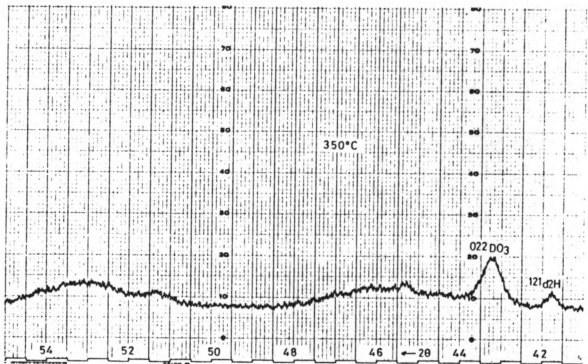
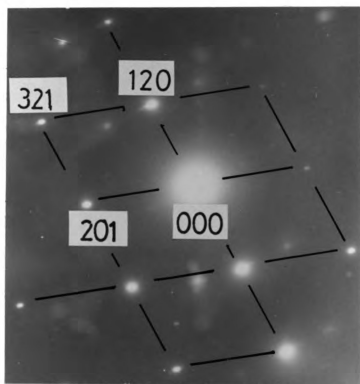


Figure 4.28 Partial diffractometer pattern of a Ni-20Cu-25Sn alloy, quenched in ice water from 1000°C, aged 24 hr at 350°C, and quenched in ice water.

Figure 4.29 Diffraction pattern of a  $[\bar{2}14]$  zone, taken from a d2H region in a Ni-20Cu-25Sn specimen, aged at 350°C for 24 hr.

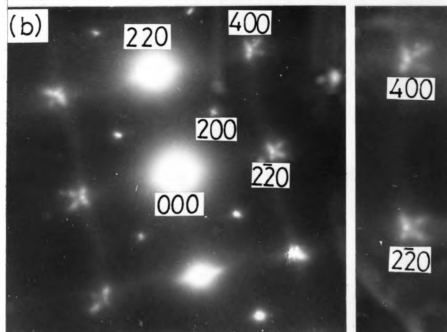
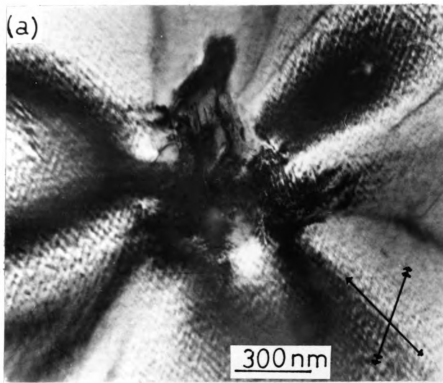


decomposition took place in the  $DO_3$  phase. This observation is discussed in further detail below.

A typical modulated structure obtained from the aged specimen is shown in Figure 4.30(a), suggesting a spinodal decomposition. A diffraction pattern taken from the same area seen in Figure 4.30(a) is shown in Figure 4.30(b). As is evident in this figure, a spinodal decomposition has occurred. The following are characteristics of the spinodal decomposition seen in Figure 4.30(b): (1) the satellite reflections, e.g., at  $2\bar{2}0$  and  $400$ , are obvious; and (2) their spacing is seen to be independent of the distance from the origin,  $000$ , as would be expected for the spinodal decomposition of a given wavelength [33]. It should be noted from the appearance of the superlattice reflections, e.g.  $200$  and  $020$ , that  $DO_3$  order is preserved despite the decomposition. This is consistent with the X-ray data shown in Table 4.2. Two more characteristics of spinodal decomposition are seen in Figure 4.30(b): (1) there are no satellites of the superlattice reflections, e.g.  $200$  and  $020$ ; and (2) no satellites of the transmission spot,  $000$ . In Figure 4.30(a), the modulated structure is seen to have two directions, which are perpendicular to the satellite reflections in Figure 4.30(b).

From the previously discussed evidence, it is apparent that the  $DO_3$  phase in the  $(Ni,Cu)_3Sn$  alloys is

Figure 4.30 Spinodal structure of a Ni-20Cu-25Sn specimen, aged 24 hr at 600°C, following ice-water quenching from 1000°C.  
(a) modulated structures of a DO<sub>3</sub> phase.  
(b) two sets of satellite reflections, perpendicular to the modulated structures.  
Note no satellite of superlattice reflections. [100] zone.



present at 600°C but it has undergone the spinodal decomposition. In this study, no further investigation was made on the spinodal structure to obtain the final structure of the decomposed phase. However, by taking the results of a recent study of (Cu,Mn)<sub>3</sub>Al alloys [34] into account, one can speculate upon the final structure.

The (Cu,Mn)<sub>3</sub>Al alloys were studied in detail by electron microscopy and diffraction analysis, and it was found that the final structure of the spinodal decomposition in these alloys was the dual structure, the DO<sub>3</sub> structure of Cu<sub>3</sub>Al and the L2<sub>1</sub> structure of Cu<sub>2</sub>MnAl [34]. Figure 4.31 shows phase relationship among M<sub>3</sub>Sn (M=Ni, Cu, and Mn) compounds. As seen in this figure, Ni-Cu-Sn alloys have both the DO<sub>3</sub> structure of Ni<sub>3</sub>Sn and the L2<sub>1</sub> structure of Cu<sub>2</sub>NiSn. From such structural similarities between the present (Ni,Cu)<sub>3</sub>Sn alloys and the (Cu,Mn)<sub>3</sub>Al alloys, it can be concluded that the final structure of the decomposed DO<sub>3</sub> phase of the (Ni,Cu)<sub>3</sub>Sn alloys would be the DO<sub>3</sub> structure of either Ni<sub>3</sub>Sn or (Ni,Cu)<sub>3</sub>Sn and the L2<sub>1</sub> structure of Cu<sub>2</sub>NiSn.

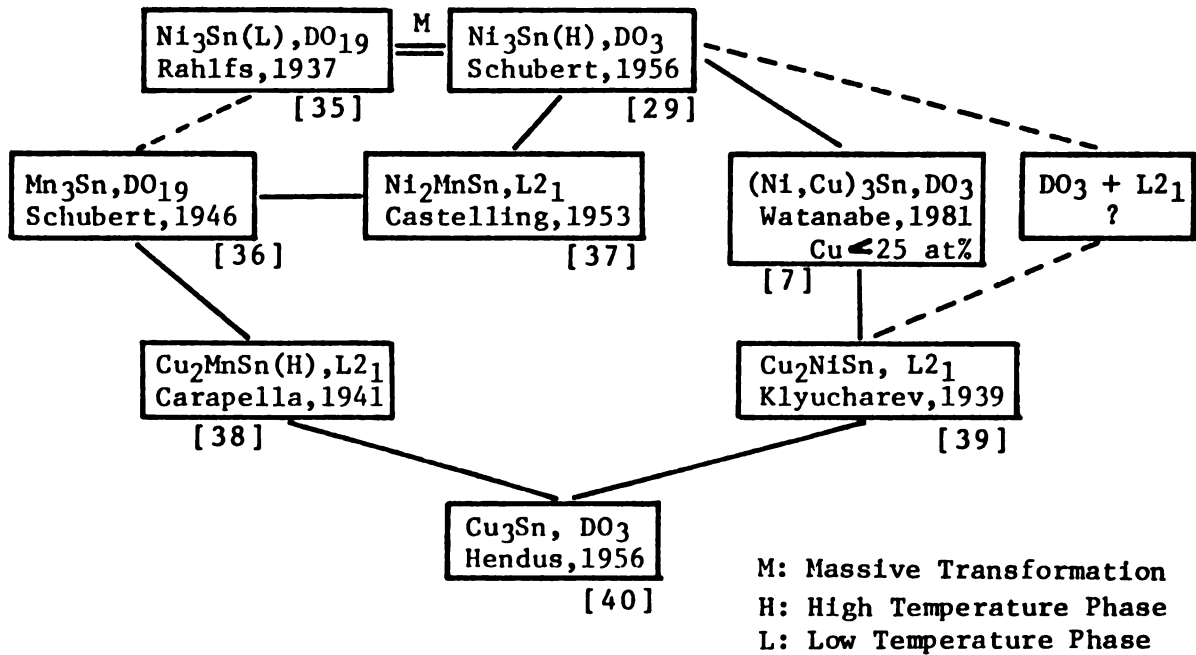


Figure 4.31 Phase relationship among  $\text{M}_3\text{Sn}$  ( $\text{M}=\text{Ni,Cu,Mn}$ ) compounds.

### 4.5.3 Conclusions Based on Aging Experiments

From the four aging experiments employed, the following conclusions can be made.

(1) the high temperature  $DO_3$  phase is stable above  $650^\circ\text{C}$  and below the melting point of the alloy ( $1022^\circ\text{C}$  measured by DTA); however, it is transformed in part to the 2H phase between 500 and  $650^\circ\text{C}$  to be the dual phases, the  $DO_3$  and 2H phases.

(2) the  $DO_3$  phase appears to be metastable at temperatures of about  $650^\circ\text{C}$ . From the appearance of the line broadening (Figure 4.28), the  $DO_3$  phase is thought to have a pre-transformation, as is often observed in many ordered martensitic alloys [41,42].

(3) the  $DO_3$  phase present in the temperature range between 500 and  $650^\circ\text{C}$  can experience a spinodal decomposition. The decomposition is believed to reach the final stage after long aging, in which the  $DO_3$  structure of the  $\text{Ni}_3\text{Sn}$  or  $(\text{Ni,Cu})_3\text{Sn}$  phase would coexist with the  $L2_1$  structure of the  $\text{Cu}_2\text{NiSn}$  phase.

(4) the d2H phase is formed at temperatures below  $500^\circ\text{C}$ .

## 4.6 Differential Thermal Analysis

### 4.6.1 Results and Discussion

To delineate the phase diagram of  $(\text{Ni,Cu})_3\text{Sn}$  alloys, a differential thermal analysis (DTA) method was used. Specimens with Cu contents of 14, 17.5, and 20 at% were examined by a DuPont Differential Thermal Analyzer after rapid quenching from  $1000^\circ\text{C}$ . These specimens were heated at a rate of  $10^\circ\text{C}/\text{min}$  in a dry argon atmosphere.

Figure 4.32a) shows a typical DTA trace obtained from a specimen with a Cu content of 14 at% Cu, whose starting phase was an as-quenched 2H martensite. In this figure, we observe four exothermic events during heating. Essentially, similar events were observed for specimens with Cu contents of 17.5 and 20 at%, although their starting phases were a retained  $\text{D0}_3$  phase. DTA traces obtained from the alloys having Cu contents of 17.5 and 20 at% are shown in Figures 4.32(b and c). To see reaction events more readily, transition temperatures seen in these three figures are tabulated in Table 4.9 along with reaction events that, we believe, took place during the heating experiments.

The first exothermic reaction took place at  $153^\circ\text{C}$  in the 14 at% Cu alloy, and at  $144^\circ\text{C}$  in the 17.5 and 20 at% Cu alloys. This reaction has widely been accepted to

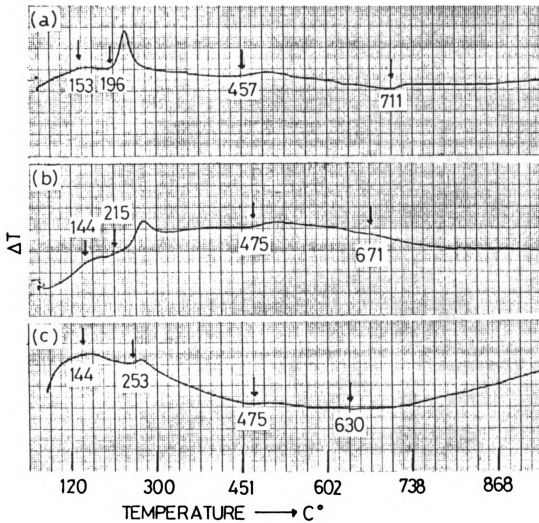


Figure 4.32  $\Delta T$ -vs- $T$  curves measured by a differential thermal analyzer in Ni-xCu-25Sn alloys during a heating process ( $\Delta T$ : temperature difference). (a)  $x=14$  at%: the starting phase being a quenched 2H martensite; (b)  $x=17.5$  at%: the starting phase being a  $\text{DO}_3$  high temperature phase; and (c)  $x=20$  at%: the starting phase being a  $\text{DO}_3$  phase.

Table 4.9 Summary of DTA analyses obtained from as-quenched  $(\text{Ni,Cu})_3\text{Sn}$  specimens

Specimen (starting phase)	Reaction temperature ( $^{\circ}\text{C}$ )	Reactions
Ni-14Cu-25Sn (2H' martensite)	153	migration of quenched-in vacancies
	196	$2\text{H}' \text{---} \rightarrow 2\text{H} + \text{d}2\text{H}$
	457	$\text{d}2\text{H} \text{---} \rightarrow 2\text{H} + \text{D}\text{O}_3$
	711	$2\text{H} \text{---} \rightarrow \text{D}\text{O}_3$
Ni-17.5Cu-25Sn (retained $\text{D}\text{O}_3$ )	144	migration of quenched-in vacancies
	215	$\text{D}\text{O}_3 \text{---} \rightarrow 2\text{H} + \text{d}2\text{H}$
	475	$\text{D}\text{O}_3 \text{---} \rightarrow 2\text{H}$
	671	$\text{d}2\text{H} \text{---} \rightarrow 2\text{H} + \text{D}\text{O}_3$ $2\text{H} \text{---} \rightarrow \text{D}\text{O}_3$
Ni-20Cu-25Sn (retained $\text{D}\text{O}_3$ )	144	migration of quenched-in vacancies
	253	$\text{D}\text{O}_3 \text{---} \rightarrow 2\text{H} + \text{d}2\text{H}$
	475	$\text{D}\text{O}_3 \text{---} \rightarrow 2\text{H}$
	630	$\text{d}2\text{H} \text{---} \rightarrow 2\text{H} + \text{D}\text{O}_3$ $2\text{H} \text{---} \rightarrow \text{D}\text{O}_3$

correspond to migration of quenched vacancies. Slight differences in the reaction temperature indicate migration energies different for various starting phases.

The second exothermic reaction started at 196°C and ended at 283°C in the 14 at% Cu alloy. This reaction is believed to correspond to the transformation from the metastable 2H martensite phase (2H') to the stable 2H and d2H phases. The second exothermic reaction observed in the 17.5 and 20 at% Cu alloys occurred at 215 and at 253°C, respectively. This reaction is considered to correspond to the transformation from the retained DO<sub>3</sub> phase to the 2H and d2H phases.

The third exothermic reaction starting at temperatures of about 457-475°C in the three alloys corresponds to the transformation from the d2H phase to the 2H and DO<sub>3</sub> phases. Between this temperature and the temperature where the fourth reaction took place, we believe that the dual phases, 2H and DO<sub>3</sub>, were formed. The fourth reaction occurred at 711°C in the 14 at% Cu alloy, at 671°C in the 17.5 at% Cu alloy, and 630°C in the 20 at% Cu alloy. This reaction corresponds to the transformation from the 2H phase to the DO<sub>3</sub> phase. Above this temperature and below melting point, all the alloys used have the single phase of DO<sub>3</sub>. By further heating the alloys with Cu contents of 14 and 20 at%, their melting points were measured to be 1112 and 1022°C, respectively.

In the DTA experiments used here, we could not detect any sign of spinodal decomposition reaction. This may be caused by a cooling rate employed, which was faster than that needed for the decomposition.

#### 4.6.2 Conclusions based on DTA Analysis

From the DTA analysis of the as-quenched alloy specimens with Cu contents of 14, 17.5, and 20 at%, the four reactions were found to have taken place below their melting points. The conclusions obtained in the present heating experiments can be summarized as follows.

[1] In the metastable 2H martensite(2H'), vacancy migration rate is highest at about 150°C, while the corresponding maximum rate occurred at about 144°C in the retained DO<sub>3</sub> phase.

[2] The 2H' martensite formed in the 14 at% Cu alloy was transformed at 200°C to the stable 2H phase and the d2H phase.

[3] The retained DO<sub>3</sub> phase was transformed to the stable 2H phase and the d2H phase at about 215°C in the 17.5 at% Cu alloy and at about 250°C in the 20 at% Cu alloy.

[4] At temperatures of about 460°C, the exothermic reaction from the d2H phase to the 2H and DO<sub>3</sub> phases took place in the three alloys with Cu contents of

14, 17.5, and 20 at%.

[5] At temperatures of around 710-630°C, the 2H phase was transformed to the DO<sub>3</sub> phase. The temperature range between this temperature and melting point is considered to be a region in which only the DO<sub>3</sub> phase is present.

## 5 DISCUSSION

### 5.1 A Proposed Phase Diagram of the (Ni,Cu)<sub>3</sub>Sn System

The X-ray and electron diffraction analyses of the alloy system have revealed that a deformed 2H phase was formed both in furnace-cooled specimens of three Ni<sub>3</sub>Sn alloys with Cu contents of 14, 17.5, and 20 at% and in specimens of the alloy with 20 at% Cu aged at 350°C. In the DTA analyses of as-quenched specimens of the three alloys, it has been suggested that, in their heating experiments, the d2H phase was transformed to the DO<sub>3</sub> and 2H phases at about 460°C. In addition to these results, the transmission electron microscopy of alloy specimens with a Cu content of 20 at% has revealed that they underwent a spinodal decomposition. The decomposition probably occurs only in the temperature range between 460 and 700°C; the former temperature corresponds to the phase boundary between a region of the DO<sub>3</sub> and 2H phases and one of the DO<sub>3</sub>, 2H, and d2H phases, according to the DTA traces; the latter temperature corresponds to the phase boundary between a single DO<sub>3</sub> region and the region of the DO<sub>3</sub> and 2H phases.

In light of all the other results obtained in the previous sections in conjunction with the above mentioned results, we can propose a new phase diagram of the

(Ni,Cu)<sub>3</sub>Sn system, which is shown in Figure 5.1. In this figure, the transition temperatures measured by the DTA method were plotted as small solid circles. As seen in this figure, the new phase diagram is quite different from Figure 1.10 proposed by Murakami et al [7-9].

In Figure 5.1 a two-phase region of DO<sub>3</sub> and L2<sub>1</sub> phases was proposed to exist in the range of Cu contents higher than 25 at%, which was based on the following X-ray data: Watanabe et al [7] reported that (Ni,Cu)<sub>3</sub>Sn alloys had the DO<sub>3</sub> structure at temperatures below their melting points for all alloys with Cu contents up to 25 at%; Klyucharev [39] found that a Cu<sub>2</sub>NiSn phase had the L2<sub>1</sub> structure.

In the temperature range between about 700 and 460°C, a region of three phases, DO<sub>3</sub>, 2H, and L2<sub>1</sub>, is proposed to

-----  
Footnote:

For the DO<sub>3</sub> structure, we can assume that Sn atoms are located at a-sites and Ni and Cu atoms are located at a-, c-, and d-sites at the same probability. Thus, the structure factors for 111 and 002 ordered reflections can be expressed as,

$$F_{200} = F_{111} = f_{\text{Sn}} - f_{\text{Ni}} - 4(f_{\text{Cu}} - f_{\text{Ni}})x_m/3$$

where  $x_m$  is the molar fraction of Cu and  $f_i$  (i=Ni, Cu, Sn) is an atomic scattering factor of the i-th atom.

On the other hand, for the L2<sub>1</sub> structure, by assuming that Sn atoms are located at a-sites, Ni atoms at c- and d-sites, and Cu atoms at b-sites, the structure factors can be expressed in the case where  $x_m$  is equal or less than 0.25 as,

$$F_{111} = f_{\text{Sn}} - f_{\text{Ni}} + 4(f_{\text{Ni}} - f_{\text{Cu}})x_m/3$$

$$F_{200} = f_{\text{Sn}} - f_{\text{Ni}} - 4(f_{\text{Ni}} - f_{\text{Cu}})x_m/3$$

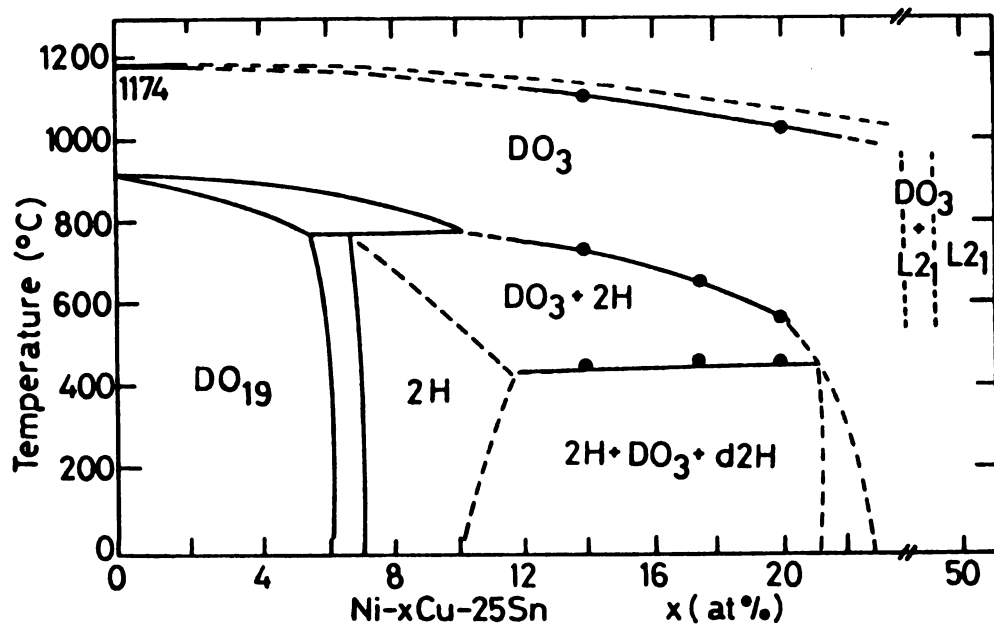


Figure 5.1 A proposed phase diagram for  $(\text{Ni,Cu})_3\text{Sn}$  alloys.

exist. Because the  $DO_3$  and  $L2_1$  structures are very similar to each other, as seen in Figure 1.1, it is not easy to differentiate them. The distinction can be made either by measuring an intensity ratio of two given ordered reflections, such as 111 and 200 (see footnote in the previous page), or by chemical analysis through analytical methods such as scanning transmission electron microscopy. Although no identification of the  $L2_1$  phase was attempted in this present study, we could observe structural evidence supporting the presence of the phase. The presence of the  $L2_1$  phase in this temperature range is considered important in reasoning for the formation of the d2H phase, which will be discussed in the next section.

## 5.2 A Formation Mechanism of a Distorted 2H Phase

Electron microscopy and DTA analysis of the specimens used in the present study have revealed that a  $DO_3$  area was transformed to both a 2H and a distorted 2H (i.e. d2H) structure. The former is an ordered orthorhombic structure (beta- $Cu_3Ti$ -type) and is a stable phase of  $(Ni,Cu)_3Sn$  alloys with Cu contents ranging between 7 and 21 at%. The same crystal structure is also seen in a martensite (2H') transformed upon rapid quenching from the  $DO_3$  phase of  $(Ni,Cu)_3Sn$  alloys with Cu contents up to 14 at%. Why the orthorhombic 2H structure was formed from the  $DO_3$  phase in these two cases is explainable by taking atom arrangements of their specific planes into account. On the other hand, the latter is an ordered triclinic structure and formation mechanisms for the lattice distortion of the d2H structure are not clear if the  $DO_3$  structure is considered as a crystal structure of the parent phase.

In this section, therefore, we will discuss a possible formation mechanism of the triclinic structure originating from the  $DO_3$  phase. This discussion will be made after relationships of atomic arrangements are described between the high-temperature  $DO_3$  phase and its three products, the stable and metastable 2H phases and the  $DO_{19}$  phase.

### 5.2.1 Relationship Among $DO_3$ , 2H, and $DO_{19}$ Structures

In Figure 5.2 are shown schematic atom arrangements of close-packed planes for  $DO_{19}$  and 2H structures of the stoichiometric  $Ni_3Sn$  alloy: (a) the (0001) basal plane of  $DO_{19}$  and (b) the (001) plane of 2H structure. By comparing Figure 5.2(b) with Figure 1.1, one can notice that the (001) plane of a 2H martensite has an atom arrangement similar to that of the (110) plane of the  $DO_3$  parent phase. This is because the transformation of the  $DO_3$  phase to the 2H martensite does not take place by diffusion of atoms but by shear motion of atoms. This transformation is known to be explained by the Burger's relation [43]. It should be noted from Figure 5.2(b) that Sn atoms are surrounded by 6 Cu atoms holding two mirror planes, perpendicular to each other: (100) and (010). From this atom arrangement and because the third axis, c-axis, is perpendicular to the (001) plane, it can be seen that the 2H structure can hold an orthorhombic symmetry. For a metastable 2H martensite formed in the alloy with a Cu content of 14 at%, an atom arrangement similar to that shown in Figure 5.2(b) is expected; in this case, Sn atoms are surrounded by a solid solution of Cu and Ni atoms randomly occupying the Ni sites in the stoichiometric alloy, resulting in an orthorhombic symmetry.

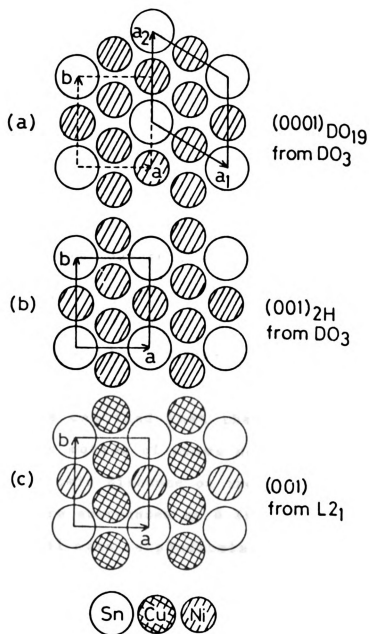


Figure 5.2 Atomic arrangements of closed-packed planes.  
 (a) the  $(0001)$  plane of  $DO_{19}$  structure;  
 (b) the  $(001)$  plane of  $2H$  structure;  
 (c) the  $(001)$  plane of  $d2H$  structure.

For a stable 2H phase formed in both furnace-cooled and aged alloys with Cu contents ranging between 7 and 20 at%, a similar situation can be seen. In this case, however, because of diffusion of atoms associated in forming this 2H phase, the following situation is possible: the compositions of Cu and Ni surrounding Sn atoms are changed during the transformation from the  $DO_3$  to the stable 2H phase but an orthorhombic symmetry remains unchanged by having a solid solution of Ni and Cu around Sn atoms. This can be seen from the phase diagram proposed in the previous section.

For the  $DO_{19}$  structure, a similar discussion can be made. This phase is massively transformed in alloys with Cu contents up to 6 at%. By comparing an atom arrangement of the (0001) plane shown in Figure 5.2(a) with that in Figure 1.1, one can find that the basal plane can be formed by shear motion of atoms on every other  $(010)_{2H}$  planes by one atomic distance on the  $(001)_{2H}$  plane. Note that Sn atoms are surrounded by 6 Ni atoms holding a six-fold symmetrical axis perpendicular to the basal plane. That is, the  $DO_{19}$  structure has a hexagonal structure but can be considered to be an orthorhombic structure. The a- and b-axes, when this orthorhombic lattice is considered, are shown in Figure 5.2(a). Comparing axial ratios of  $b/a$  for the 2H and  $DO_{19}$  structures, one can notice that the 2H structure is slightly distorted from the hcp symmetry.

### 5.2.2 Formation of d2H from $DO_3$ via $L2_1$

The above mentioned examples show that the orthorhombic symmetry of the 2H and  $DO_{19}$  structures can be derived from the atom arrangements of the (110) plane of the  $DO_3$  structure. This suggests that the parent phase of the d2H should not be the  $DO_3$  phase. Further distortion from the 2H lattice, when the d2H lattice is formed, can be explained based on the assumption that some compositional changes occur in the vicinity of  $DO_3$  regions wherein the stable 2H phase is formed.

As discussed in the previous section, an  $L2_1$  phase can be transformed from the high-temperature  $DO_3$  phase by the following processes: 1) a spinodal decomposition of the  $DO_3$  phase, and 2) a diffusion process associated with the formation of an Ni-rich 2H phase. The former process would not occur in the case when specimens are furnace-cooled, while the latter process seems more plausible.

Figure 5.3 shows schematic illustrations describing the formation process of a region of  $L2_1$  structure. As shown in the phase diagram (Figure 5.1), a specimen of the  $DO_3$  structure is stable at temperatures higher than about  $760^\circ\text{C}$ . As soon as the temperature of the specimen is lowered below  $760^\circ\text{C}$ , stable 2H regions start to form from the  $DO_3$  phase. These 2H regions should be Ni-rich, and consequently, areas surrounding them become Ni-poor

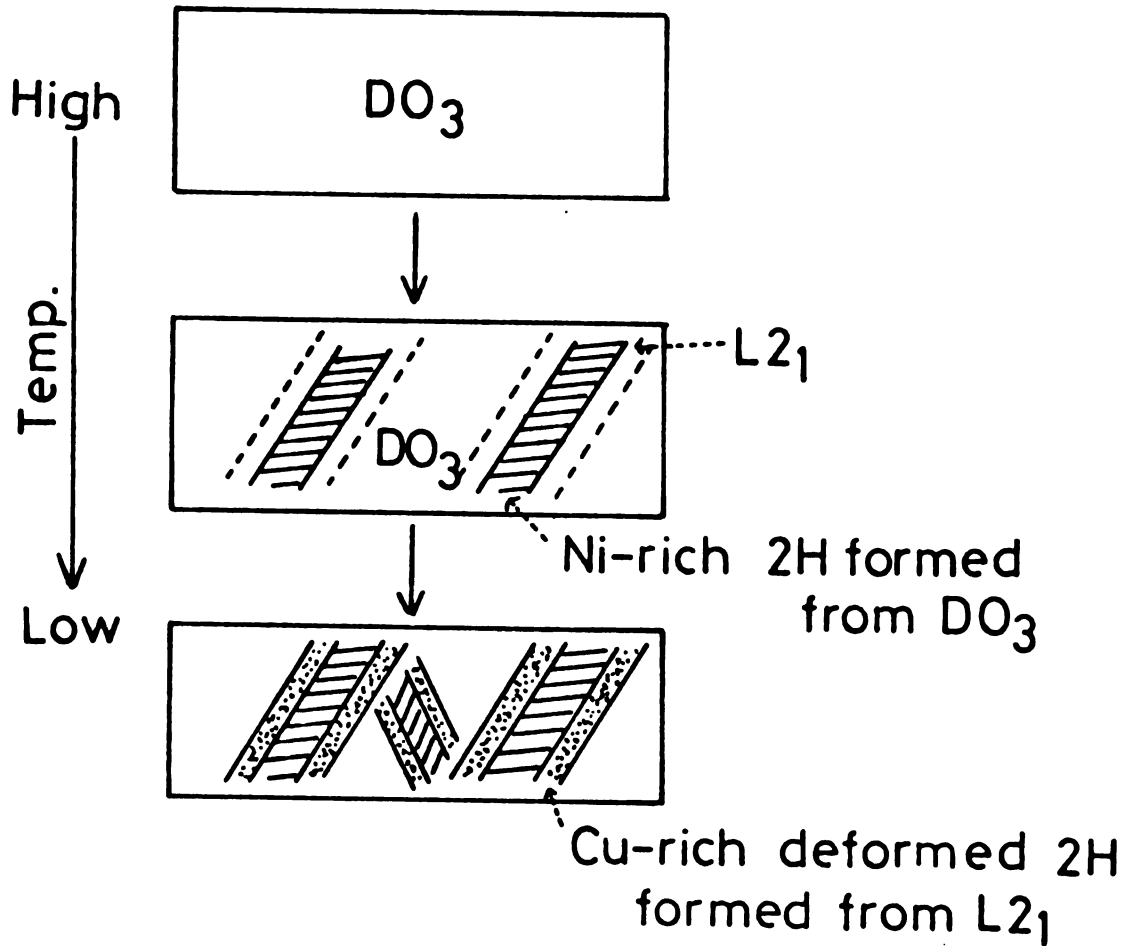
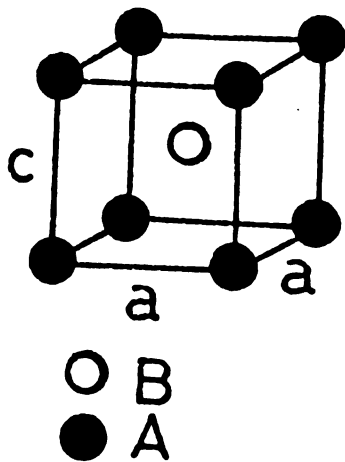


Figure 5.3 Schematic illustration describing a formation process of a d2H from  $DO_3$  via  $L2_1$ .

and Cu-rich. The resultant Cu-rich areas can change or can be transformed to the  $L2_1$  phase, because this structure bears great resemblance to the  $DO_3$  structure. When the temperature is further lowered below  $470^\circ\text{C}$ , a new phase is formed in the  $L2_1$  region and can be distorted due to an atom arrangement of the (001) plane of the new (i.e. d2H) phase because of the following reason.

Figure 5.2(c) shows such an atom arrangement of the (001) plane of the d2H structure. Comparing Figures 5.2(a, b, and c), one can notice that the crystal symmetry of the basal plane becomes the highest for the  $DO_{19}$  structure and the lowest for the d2H structure. Although the two-fold symmetry of the  $(001)_{2H}$  plane still remains unaltered in the (001) plane of the d2H phase, a further distortion from the 2H lattice is considered to take place in Figure 5.2(c). It is well known that some alloys such as VIr and MnAu[44] have a tetragonality from CsCl-type structure even though they have high lattice symmetry as long as the rigid atom model is concerned (Table 5.1). Therefore, it is likely that the crystal structure formed from the  $L2_1$  phase can undergo further lattice distortion, resulting in the triclinic structure of the d2H phase.

Table 5.1 Examples of tetragonally distorted CsCl-type compounds.



VRu	$c/a = 1.04$
VIr	$c/a = 1.34$
TiRh	$c/a = 1.14$
TiIr	$c/a = 1.17$
MnAu	$c/a = 0.95$
ZnNi	$c/a = 1.16$

## 6 SUMMARY AND CONCLUSIONS

The phase transformations in  $(\text{Ni,Cu})_3\text{Sn}$  alloys were investigated in detail by optical and scanning and transmission electron microscopy, electron and X-ray diffraction techniques, and differential thermal analysis. The alloys used were the ones containing Cu contents ranging between 10 and 22 at%. The results obtained in this study can be summarized as follows:

[1] Specimens of alloys with Cu contents of 14, 17.5, and 20 at% were furnace-cooled from  $1000^\circ\text{C}$  and it was found that those specimens showed the presence of two phases. One was the most abundant phase, exhibiting rod-shaped microstructures, and the other was the less abundant phase, exhibiting very fine acicular structures. Electron and X-ray diffraction analyses and electron microscopy manifested that the former phase had an ordered 2H (beta- $\text{Cu}_3\text{Ti}$ -type) orthorhombic structure, containing (101) faults and a low density of dislocations. The latter phase was identified to have a triclinic structure, slightly distorted from the 2H structure, denoted as d2H. The acicular structures of this d2H phase contained a large number of uniformly distributed internal planar faults. The lattice parameters measured of the d2H phase were  $a=4.53\text{\AA}$ ,  $b=5.31\text{\AA}$ ,  $c=4.34\text{\AA}$ ,  $\alpha=85^\circ$ ,  $\beta=86^\circ$ , and  $\gamma=84^\circ$ . X-ray diffraction analyses showed that the three phases of 2H, d2H, and  $\text{DO}_3$  were present in furnace-

cooled specimens.

[2] Several  $(\text{Ni,Cu})_3\text{Sn}$  alloys were quenched from  $1000^\circ\text{C}$  to ice water. It was found that a high-temperature  $\text{DO}_3$  phase was retained for as-quenched specimens containing Cu contents ranging from 16 and 22 at%. This observation disagrees with results obtained by Murakami et al [7-9] who reported that the high-temperature phase was transformed to a 2H martensite. In this study, such a 2H martensite was only observed in specimens with a Cu content of 14 at%. This martensite was found to contain (121) twins.

[3] Aging experiments of a  $\text{Ni}_3\text{Sn}$  alloy containing a Cu content of 20 at% were carried out for 24 hr at temperatures of 350, 500, 600, and  $650^\circ\text{C}$ . From the four aging experiments, the following conclusions can be made.

(a) The high temperature  $\text{DO}_3$  phase was stable above  $650^\circ\text{C}$  and below the melting point ( $1022^\circ\text{C}$ ) of this alloy; however, this phase was transformed in part to the 2H phase between 500 and  $650^\circ\text{C}$  to be the dual phases, the  $\text{DO}_3$  and 2H phases.

(b) The  $\text{DO}_3$  phase appears to be metastable at temperatures of about  $650^\circ\text{C}$ . From the appearance of the X-ray line-broadening, the  $\text{DO}_3$  phase is considered to have a pre-transformation, as is often observed in many ordered martensitic alloys.

(c) The  $\text{DO}_3$  phase present in the temperature range

between 500 and 650°C can experience a spinodal decomposition. The decomposition is believed to reach the final stage after long aging, in which the DO<sub>3</sub> structure of the Ni<sub>3</sub>Sn or (Ni,Cu)<sub>3</sub>Sn phase would coexist with the L2<sub>1</sub> structure of the Cu<sub>2</sub>NiSn phase.

(d) The d2H phase should be formed at temperatures below 500°C.

[4] From differential thermal analyses and electron diffraction analyses, the following results were obtained. The high-temperature DO<sub>3</sub> phase was transformed to an ordered 2H (beta-Cu<sub>3</sub>Ti-type) orthorhombic phase at temperatures ranging between 710 and 630°C in alloys containing Cu contents between 14 and 20 at%. Residual areas of the DO<sub>3</sub> phase were then transformed to both the 2H phase and the d2H phase at a temperature of around 460°C.

[5] Based on the experimental results obtained in this study, a new phase diagram was proposed for the (Ni,Cu)<sub>3</sub>Sn alloys in the range of Cu contents between 10 and 22 at%. This phase diagram was different from the one available in literature, which shows a single phase of 2H at temperatures below about 900°C in the range of Cu contents between 8 and 18 at%.

[6] It is proposed that the d2H phase is formed at about 460°C from an L2<sub>1</sub> phase which is considered to be transformed in residual DO<sub>3</sub> regions neighboring 2H areas.

## REFERENCES

- 1) S. Rosen, J. A. Geobel: Trans. AIME, 242(1968), 722.
- 2) K. Enami, S. Nenno, and K. Shimizu: Trans. JIM, 14(1972), 161.
- 3) J. L. Smialek and R. H. Heheman: Met. Trans, 4(1973), 1571.
- 4) S. Chakravorty and C. M. Wayman: Met. Trans., 7A(1976), 569.
- 5) Y. Murakami and S. Kachi: Trans. JIM, 18(1977), 423.
- 6) H.-r. Pak, T. Saburi, and S. Nenno: Trans. JIM, 37(1973), 1128.
- 7) Y. Yatanabe, Y. Murakami, and S. Kachi: Trans. JIM, 6(1981), 551.
- 8) Y. Murakami and S. Kachi: Trans. JIM, 24(1983), 9.
- 9) Y. Murakami and S. Kachi: Trans. JIM, 24(1983), 747.
- 10) K. Otsuka, T. Sawamura, and K. Shimizu: Phys. Stat. Sol, (a) 5(1971), 457.
- 11) K. Otsuka and K. Shimizu: Phil. Mag., 24(1971), 481.
- 12) D. B. Masson and C. S. Barrett: Trans. AIME, 212(1958), 260.
- 13) D. B. Masson: Trans. AIME., 218(1960), 64.
- 14) L. C. Chang: Acta Cryst., 4(1951), 320.
- 15) R. S. Toth and H. Sato: Acta Metall., 16(1968), 413.
- 16) P. L. Ferraglio and K. Mukherjee: Acta Metall., 22(1974), 835.
- 17) T. B. Massalski and H. W. King: Progress in Materials Science, 10(1961), 1.
- 18) H. Sato: Met. Soc. Conf., 29(1963), 295.
- 19) H. Sato, R. S. Toth, and G. Honjo: Phys. Chem. Solid, 28(1967), 137.
- 20) S. Kajiwara: J. Phys. Soc. Japan, 22(1967), 795.

- 21) A. B. Greninger: Trans. AIME., 133(1939), 204.
- 22) T. B. Massalski: Acta Metall., 6(1958), 243.
- 23) J. E. Kittl and T. B. Massalski: Acta Metall., 15(1967), 161.
- 24) K. H. G. Ashbee, L. F. Vassamillet, and T. B. Massalski: Acta Met., 15(1967), 181.
- 25) T. Saburi and C. M. Wayman: Trans. AIME, 233(1965), 1373.
- 26) J. F. Kittl and C. Rodriguerz: Acta Metall., 17(1969), 925.
- 27) M. Hansen and K. Anderko: Constitution of Binary Alloys, McGraw-Hill, New York, (1958), 1042.
- 28) O. Nial: Svensk Kem. Tidskr., 59(1947), 172.
- 29) K. Schubert, P. Esslinger, E. Gunzel, G. Meissner, W. Schtt, J. Wegst, and M. Wilkens: Naturwiss, 43(1956), 248.
- 30) S. N. Chang: Matser Thesis, MSU, 1983.
- 31) H.-r. Pak, S. N. Chang, and M. Kato: J. Mat. Sci., 20(1985), 947.
- 32) K. Osuka and K. Shimizu: Jap. J. Appl. Phys., 8(1969), 1196.
- 33) H. Kubo, I. Cornels, and C. M. Wayman; Acta. Metall., 28 (1980), 405.
- 34) M. Bouchard and G. Thomas; Acta Metall., 23(1975), 1485.
- 35) P. Rahlfs: Metallwirtschaft, 16(1937), 343.
- 36) H. Nowotny and K. Schubert: Z. Metallkde, 37(1946), 17.
- 37) L. Castelling: Mh. Chem., 84(1953), 765.
- 38) L. A. Carapella and R. Hultgren: Phys. Rev., 59(1941), 905.
- 39) A. P. Klyucharev: Z. Eksper. Teort. Fiz., 9(1939), 1501.
- 40) H. Hendus and H. Knodler: Acta Cryst., 9(1956), 1036.

- 41) L. Delaey, A.J. Perkins and T.B. Massalski:  
J. Mat. Sci., 7(1972), 1197.
- 42) C. M. Wayman: Mat. Res. Soc. Symp. Proc.,  
39(1985), 77.
- 43) W. G. Burgers: Physica, 1(1934), 561.
- 44) A. E. Dwight: Intermetallic Compounds, ed. J.H.  
Westbrook, John Wiley & Sons, Inc., NY, 1967.